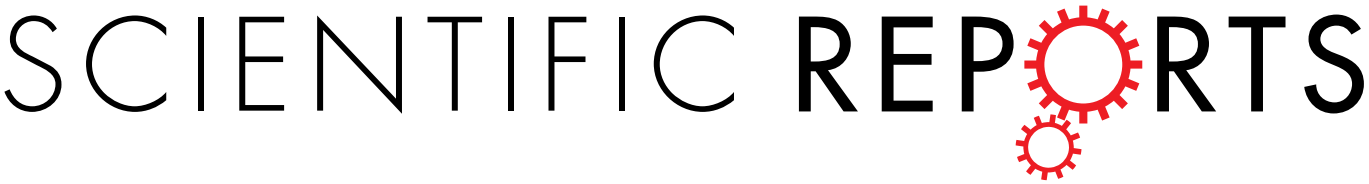

OPEN

Alterations in voltage-sensing of the mitochondrial permeability transition pore in ANT1-deficient cells

Received: 10 May 2015
Accepted: 09 May 2016
Published: 25 May 2016

Judit Doczi[1,2], Beata Torocsik[1], Andoni Echaniz-Laguna[3], Bénédicte Mousson de Camaret[4], Anatoly Starkov[5], Natalia Starkova[6], Aniko Gál[7], Mária J Molnár[7], Hibiki Kawamata[5], Giovanni Manfredi[5], Vera Adam-Vizi[1] & Christos Chinopoulos[1,2]

The probability of mitochondrial permeability transition (mPT) pore opening is inversely related to the magnitude of the proton electrochemical gradient. The module conferring sensitivity of the pore to this gradient has not been identified. We investigated mPT's voltage-sensing properties elicited by calcimycin or H_2O_2 in human fibroblasts exhibiting partial or complete lack of ANT1 and in C2C12 myotubes with knocked-down ANT1 expression. mPT onset was assessed by measuring *in situ* mitochondrial volume using the 'thinness ratio' and the 'cobalt-calcein' technique. De-energization hastened calcimycin-induced swelling in control and partially-expressing ANT1 fibroblasts, but not in cells lacking ANT1, despite greater losses of mitochondrial membrane potential. Matrix Ca^{2+} levels measured by X-rhod-1 or mitochondrially-targeted ratiometric biosensor 4mtD3cpv, or ADP-ATP exchange rates did not differ among cell types. ANT1-null fibroblasts were also resistant to H_2O_2-induced mitochondrial swelling. Permeabilized C2C12 myotubes with knocked-down ANT1 exhibited higher calcium uptake capacity and voltage-thresholds of mPT opening inferred from cytochrome c release, but intact cells showed no differences in calcimycin-induced onset of mPT, irrespective of energization and ANT1 expression, albeit the number of cells undergoing mPT increased less significantly upon chemically-induced hypoxia than control cells. We conclude that ANT1 confers sensitivity of the pore to the electrochemical gradient.

Mitochondria that are subject to calcium overload exhibit a permeability transition mediated by a pore forming in the inner mitochondrial membrane[1,2]. The identity of the structural components of this pore has been until recently unknown; in the past three years though, the c-rings of the ATP synthase[3,4], and the interface within ATP synthase dimers[5] are being strongly favoured for filling this gap of knowledge[6,7,2], but still with a number of questions unanswered, reviewed in[8–10]. Nonetheless, over the past three decades extensive amount of efforts have focused on the regulation and functional characteristics of this phenomenon[11], and an inverse correlation of the probability of pore opening to the magnitude of the electrochemical gradient has been thoroughly characterized[12–15]. The molecular entity responsible for the voltage-dependence of the pore has not been identified, though the tuning of this sensor by the oxidation-reduction state of vicinal thiols as well as the contribution of critical arginines has been reported[16–19]. Relevant to this, glutathione depletion in cultured neurons by monochlorobimane was shown to initiate bioenergetic deficiency that was mediated by inhibition of ANT[20]. ANT exhibits a number of thiols that are amenable to oxidation by several agents[21,22], some of which are unmasked in

[1]Department of Medical Biochemistry, Semmelweis University MTA-SE Laboratory for Neurobiochemistry, Budapest, 1094, Hungary. [2]MTA-SE Lendület Neurobiochemistry Research Group, Budapest, Hungary. [3]Département de Neurologie, Hôpitaux Universitaires, Hôpital de Hautepierre, 67098 Strasbourg cedex, France. [4]Service des Maladies Héréditaires du Métabolisme, Centre de Biologie et de Pathologie Est, CHU Lyon, 69677 Bron cedex, France. [5]Feil Family Brain and Mind Research Institute, Weill Cornell Medical College, New York, NY 10065, USA. [6]Icahn School of Medicine at Mount Sinai, Department of Hematology and Medical Oncology, New York, NY 10029, USA. [7]Institute of Genomic Medicine and Rare Disorders, Semmelweis University, Budapest, 1083, Hungary. Correspondence and requests for materials should be addressed to C.C. (email: chinopoulos.christos@eok.sote.hu)

an energy-dependent manner[23]. Strong circumstantial evidence led to the formulation of the theory that the ANT is a structural part of the pore[24], backed by hundreds of publications showing impacts of all known ANT ligands on pore opening probability[25].

However in 2004, the Wallace's group showed that in the livers of genetically modified mice in which both isoforms of ANT were inactivated, mitochondria still exhibited Ca^{2+}-induced pore opening albeit requiring higher amounts of Ca^{2+} loading, and that the effects of ANT ligands were completely abolished[26]. From this report alone, the ANT was deemed as modulatory but not structural component of the mPT. On the other hand, mitochondria obtained from the crustacean *Artemia franciscana* do not exhibit a calcium-regulated pore in view of profound calcium storage[27], an organism that was recently shown to expresses a unique ANT being refractory to bongkrekic acid[28], a dual inhibitor for ANT and mPT[29]. Yet, ANTs expressed in related crustacean organisms that lack a Ca^{2+}-induced mPT, exhibited sensitivity of ANT-mediated adenine nucleotide exchange to bongkrekic acid[30], while allogenic expression of Artemia ANT in yeasts also conferred sensitivity to this poison[31].

Mindful of the above, one may conclude that the ANT is not a structural element of the pore, however, the involvement of this transporter in the regulation of the mitochondrial permeability transition is more than likely. Hereby we investigated the response of *in situ* mitochondria in intact cells lacking partially or completely ANT1 to Ca^{2+}-induced mPT opening conferred either by i) the Ca^{2+}-ionophore calcimycin or ii) H_2O_2, and as a function of the proton electrochemical gradient, also distinguishing between high- *vs* no electron flow in the respiratory chain. We also investigated the voltage thresholds of inducing mPT by submaximally loading permeabilized cells with calcium, and titrating mitochondrial membrane potential with cyanide or an uncoupler. Our results show that ANT1 is the voltage-sensor of the mPT, in line with earlier firm evidences proposing ANT as the voltage-sensor of the pore, as well as being the site of action of oxidative stress[24,32,33].

Results

Effect of loss of ANT1gene expression on *in situ* mitochondrial swelling induced by calcimycin in human fibroblasts at different bioenergetic states. The patient (AF) exhibited a complete loss of *ANT1* expression gene due to a homozygous G to A substitution ($c.111 + 1G > A$) abolishing the invariable consensus GT splice donor site of intron 1[34]. The patient suffered from cardiomyopathy and myopathy, while her heterozygote mother (ST) was free from these clinical symptoms. In cultured fibroblasts from the patient, mitochondria appeared to be normal under ultrastructural examination and there were no alterations in the activities of respiratory chain complexes; mtDNA rearrangements or increased mtDNA copy number were absent. A thorough description of the clinical case, histopathological and biochemical findings in muscle and cultured fibroblasts appear in ref. 34. Regarding the fibroblasts from the individuals that were used in our study, ST exhibited a faint band of mRNA coding for ANT1, while AF fibroblasts exhibited no band of mRNA coding for this isoform, in northern blotting (panel Fig. 1A,B). mRNA coding for ANT2 appeared to be unaffected (see below under qPCR evaluation). Western blotting analysis (panel Fig. 1C) showed that patient AF had no detectable expression of ANT1, while the heterozygous mother exhibited moderate ANT1 protein expression. On the contrary, ANT2 protein expression was slightly elevated in AF cells compared to either ST cells or the three controls.

Swelling of AF, ST and three control subjects' mitochondria within fibroblasts were compared during Ca^{2+} overload, induced by addition of calcimycin (4Br-A23187, 2 μM). Although the impact of calcium ionophores on *in situ* mitochondria has not been attributed to the permeability transition in at least one study[35], there, the effect of the ionophore was not studied for more than 10 minutes. On the other hand, induction of the mPT in *in situ* mitochondria has been succesfully employed in many other cell models, for more extended periods of time[15,36–40], as in the present study. The bathing solution of the cells was deprived of Mg^{2+} because calcimycin conducts Ca^{2+} and Mg^{2+} almost equally well. Understandably, mitochondrial swelling in a Ca^{2+}-containing but Mg^{2+}-free medium may be due to opening of the inner membrane anion channel "IMAC"[41] and/or K^+-uniport[42], in addition to that attributed by the mPT; however, the first two mechanisms operate in all five cell lines, and thus would not serve as confounding factors in the results obtained due to differences in ANT1 expression. Mitochondria were visualized by wide field epifluorescence imaging of either i) mitochondrially targeted DsRed2, or ii) mitochondrially trapped calcein while cytoplasmic calcein fluorescence was quenched by cobalt (see below), a method devised by Petronilli *et al.*[43]. Swelling monitored by evaluating DsRed2-visualized mitochondrial morphology and changes in mean mitochondrial diameters were calculated using the thinness ratio technique, a methodology devised by Gerencser *et al.*[44]. In these assays the onset of swelling was defined by a sudden decrease in the thinness ratio, δTR. A representative epifluorescence image before and after induction of mPT are shown in panel Fig. 1D. A time-lapse series of such experiments are shown in the Supplemental Material, as a function of metabolic conditions (mPT_DsRed2_control_HF_calcimycin_plus_Glc.avi, mPT_DsRed2_control_HF_calcimycin_no_Glc_plus_CN.avi, and mPT_DsRed2_control_HF_calcimycin_no_Glc_plus_UNC.avi). A representative thinness ratio trace is shown in panel Fig. 1E, calculated from the recorded time-series images. In the experiments performed with AF, ST and control subjects' cells during various metabolic conditions described below, the following parameters were recorded: i) the time elapsed from the addition of calcimycin to the appearance of a large magnitude swelling (marked as 'onset to mPT', panel Fig. 1F) ii) the amplitude of swelling (marked as 'δTR amplitude', panel Fig. 1G), and iii) the number of cells exhibiting the large magnitude swelling considered as mPT within the experimental time frame (4 hours in the presence of 2 μM calcimycin), depicted in panel Fig. 1H.

As shown in panel Fig. 1F, the calcimycin-induced swelling of *in situ* ST (black bars) mitochondria was hastened by glucose deprivation and NaCN co-application (p-value $a^* = 0.027$, t-test); likewise, swelling of *in situ* mitochondria of two out of the three control subjects' cells (white bars) was hastened by glucose deprivation and NaCN co-application (p-value: $b^* = 0.005$, t-test and $c^* = 0.04$, t-test). This is consistent with the findings on mouse mitochondria reported previously by our group[15], and in line with the established phenomenon that a diminished electrochemical gradient primes mitochondria to undergo Ca^{2+}-induced mPT. However, the calcimycin-induced swelling of *in situ* AF (grey bars) mitochondria was delayed, compared to other cell types

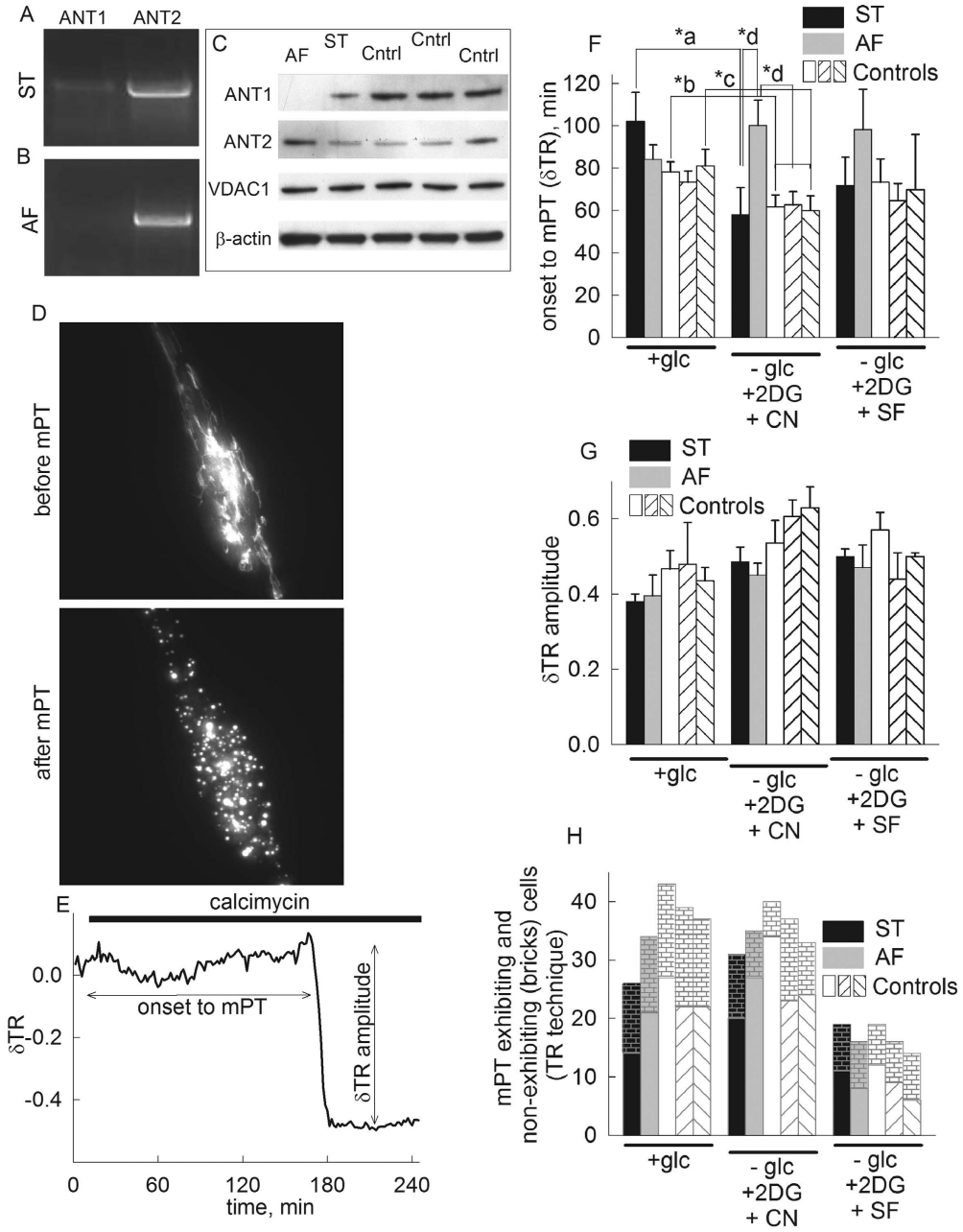

Figure 1. Effect of loss of *ANT1* gene expression on *in situ* mitochondrial swelling (visualized by DsRed2) induced by calcimycin in human fibroblasts during various metabolic conditions [+ glucose, no glucose + 2-deoxyglucose (2 mM) + NaCN (5 mM), no glucose + 2-deoxyglucose + SF 6847 (SF, 1 μM), detailed in the y-axis of the panels]. (**A**) Northern blot image of ST cells for ANT1 and ANT transcripts. (**B**) Northern blot image of AF cells for ANT1 and ANT2 transcripts. (**C**) Scanned images of Western blots of AF, ST and control cells from three healthy donors (35 μg loading per lane) directed against ANT1, ANT2, VDAC1 and β-actin. (**D**) Epifluorescence image of a fibroblast transfected with DsRed2 before and after induction of mPT. (**E**) Representative trace of the effect of calcimycin (2 μM) on the thinness ratio (δTR) indicating mitochondrial volume as a function of time. (**F**) Time elapsed between calcimycin application and mitochondrial swelling (onset to mPT) detected by wide field imaging of mito-DsRed2 expressed in cultured fibroblasts from the heterozygous mother (ST, black bars) the patient (AF, grey bars), and three control subjects (white bars) during various metabolic conditions, detailed under the x-axis. The onset to mPT was determined by the sudden increase of mean mitochondrial diameter in the microscopic view field described as a sudden decrease of the thinness ratio (δTR). Bars indicate means ± S.E.M. of 14–43 cells from at least 8 different cultures as detailed in panel 1D (*$p < 0.05$ significance by Student's t-test for 'a' 'b' and 'c' or ANOVA 'd'; p-values: *a = 0.027, *b = 0.005, *c = 0.04, *d = 0.027. (**G**) Quantification of the δTR amplitude (as marked in panel F) for AF vs ST vs control cells during various metabolic conditions, detailed on the x-axis. (**H**) Comparison of mPT-exhibiting and non-exhibiting cells (bricks) in fibroblasts from ST (black bars), AF (grey bars) and control subjects (white bars) with the TR technique during various metabolic conditions, detailed on the x-axis, using Fisher exact test.

during glucose deprivation and NaCN co-application (p-value: $d^* = 0.027$, one-way ANOVA); furthermore, this parameter was not statistically significantly different from the other cell types during energized conditions. Although the above tendencies were the same for ST and AF cells during glucose deprivation and co-application of the uncoupler SF 6847 compared to the fully energized state, no statistically significant difference was reached.

Within the 4 hours of the experimental time frame the amplitude of swelling (panel Fig. 1G) was not significantly different between ST, AF or control cells under any metabolic condition. This is important, because different cell types exhibit different amplitudes of swelling, for unknown reasons[44]. The absence of a difference in these amplitudes among AF, ST and control cell mitochondria imply that the absence of ANT1 in AF cells did not confer a large, confounding alteration, thus supporting the notion that the mechanism of swelling must be the same for all cells, likely the opening of the permeability transition pore. Accordingly, as shown in panel Fig. 1H, the number of cells exhibiting large-magnitude swelling within the 4 hours of the experimental time frame was also not statistically significant among any cell type.

Visualization of DsRed2-expressing mitochondria offers superior imaging quality and the fluorescent protein does not exit mitochondria upon swelling. However, transfection efficiency is very low, typically less than 5% in fibroblasts. Therefore, we complemented this approach with the cobalt-calcein technique, a method that outlines the mitochondrial network of all cells. On the other hand, the amount of calcein loading has to be carefully titrated, as it may be toxic to the cells, plus mitochondrially-trapped calcein fluorescence is lost rapidly after opening of the mPT. In our hands, 50 nM of calcein-AM loading at 4 °C was optimal; below this concentration the signal-to-noise ratio was unsatisfactory, while above 100 nM mitochondria from all cell types fragmented a few minutes after loading. Representative epifluorescence images of cells before and after induction of mPT are shown in panel Fig. 2A,B, respectively. A time-lapse series of such an experiment is shown in the Supplemental Material (mPT_COBCA_control_HF_calcimycin_plus_Glc.avi). The thinness ratio technique cannot be applied on calcein-loaded mitochondria, so therefore organellar volume cannot be quantified; using the cobalt-calcein method we only investigated the time elapsing from addition of calcimycin to transformation of mitochondria from a thread-to-ball configuration followed by immediate loss of calcein fluorescence, implying mPT opening. Furthermore, we only investigated the effect of glucose (fully energized state) versus no glucose plus 2-deoxyglucose plus NaCN (fully de-energized state, no electron flow), because the uncoupler SF 6847 was rapidly quenching mitochondrially-trapped calcein fluorescence. The time elapsed until onset of mPT assessed by the cobalt-calcein technique (cob-calc) was less than that assessed by the thinness ratio technique (compare panel Fig. 1F with 2C), in the energized state; this likely reflects the toxicity of loading with calcein. Nevertheless, as shown in panel Fig. 2C, the calcimycin-induced swelling of *in situ* AF (grey bars) mitochondria was delayed, compared to other cell types during glucose deprivation and NaCN co-application (p-value: $e^* = 0.002$, one-way ANOVA). The time elapsed until mPT onset of *in situ* AF (grey bars) mitochondria was also significantly increased in the de-energized compared to the energized state (p-value: $f^* = 0.008$, t-test). The same tendency was observed in the experiments with DsRed2-transfected cells. Similar to the results obtained from DsRed2-expressing mitochondria, as shown in panel Fig. 2D, the number of cells exhibiting loss of mitochondrially-entrapped calcein fluorescence within the experimental time frame was also not statistically significant among any cell type. From the above data we concluded that the absence of ANT1 *increased* the elapsed time to mPT opening upon calcimycin addition only during the de-energized state.

Effect of complete loss of ANT1 gene expression on matrix Ca^{2+} accumulation upon treatment with calcimycin. To show that application of calcimycin to cells leads to matrix Ca^{2+} accumulation irrespective of the de-energization treatment and to address the possibility that the alterations seen in the elapsed time to mPT upon calcimycin addition between the cell lines (results obtained from the control cell lines were pooled) could be affected by alterations in the accumulation of Ca^{2+} in the mitochondrial matrix, we evaluated matrix Ca^{2+} levels by i) mitochondrially trapped X-rhod-1 (K*d* for $Ca^{2+} = 0.7\,\mu M$) and ii) genetically encoded, mitochondrially-targeted, ratiometric calcium biosensor that contains enhanced CFP and circularly permuted Venus 173, 4mtD3cpv[45], (K*d* for $Ca^{2+} = 0.6\,\mu M$). This FRET-based ratiometric indicator exhibits a nearly exclusive preference for the mitochondrial compartment compared to X-rhod-1 distribution (not shown), though this methodology suffers from low transfection efficiency (typically less than 5%). On the other hand, with X-rhod-1 we could evaluate more cells, but the fluorescence signal could also be partially originating from the cytosolic compartment.

Mitochondrial matrix Ca^{2+} accumulation was induced in the various fibroblasts lines in the same manner as for the 'thinness ratio', while cells were either loaded with X-rhod-1 (panel Fig. 3A,C,E) or transfected with pcDNA-4mtD3cpv (panel Fig. 3B,D,F). As seen in panel Fig. 3A, representative traces (grey) of X-rhod-1 fluorescence signal representing matrix Ca^{2+} of *in situ* mitochondria are shown from a typical experiment; upon addition of calcimycin ($2\,\mu M$), there is a gradual elevation in X-rhod-1 fluorescence that reaches a plateau within 30 minutes. The mean trace with S.E.M. bars is shown superimposed in black. In panel Fig. 3B, a representative trace of 4mtD3cpv FRET ratio fluorescence is shown, in response to addition of calcimycin. From such experiments we evaluated matrix Ca^{2+} levels in the various cell lines during the exact metabolic conditions as indicated for panel Fig. 1F, with the following two parameters: i) the rate of change in X-rhod-1 and 4mtD3cpv FRET ratio fluorescence within the first 10 minutes upon addition of calcimycin, and ii) the plateau of X-rhod-1 and 4mtD3cpv FRET ratio fluorescence reached within one hour upon addition of calcimycin. The results of the first parameter are shown in panel Fig. 3C,D and for the second parameter in panel Fig. 3E,F for X-rhod-1 and 4mtD3cpv FRET ratio fluorescence, respectively. All of the results shown in Fig. 3 imply that there is a substantial elevation in matrix Ca^{2+} concentration induced by calcimycin even in the presence of cyanide or uncoupler. However, there was a statistically significant decrease in matrix Ca^{2+} accumulation recorded by 4mtD3cpv FRET ratio fluorescence (panel Fig. 3D) in AF cells compared to ST ($p = 0.044$) and control fibroblasts ($p = 0.042$) during de-energization by cyanide. No statistically significant difference was recorded for any other comparison.

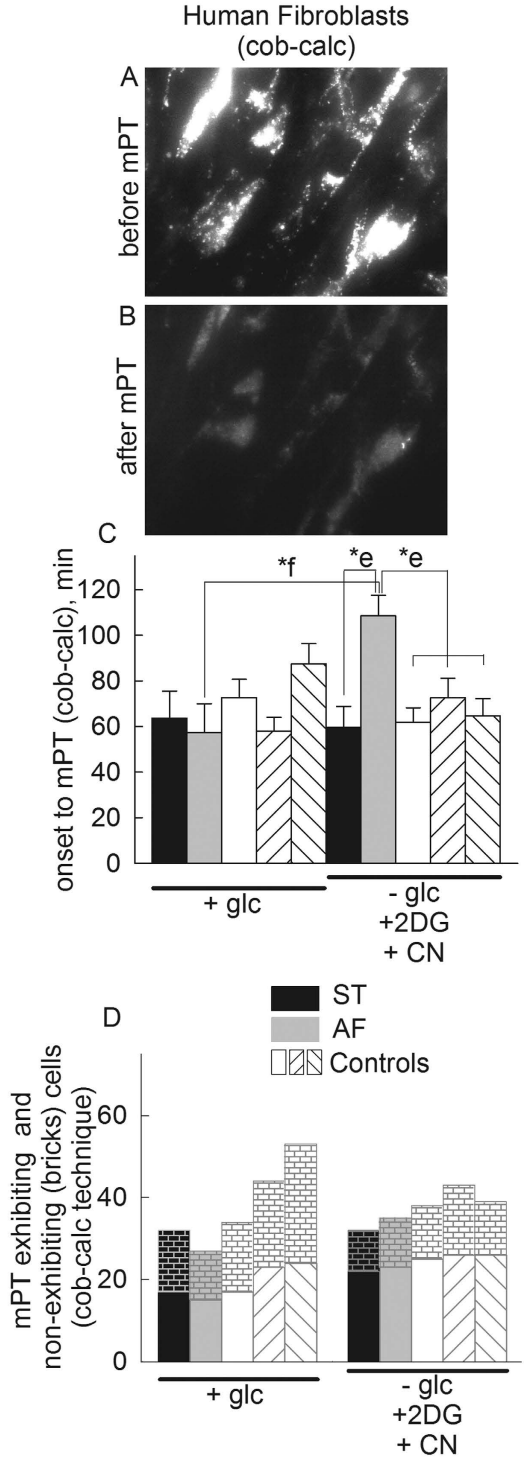

Figure 2. Effect of loss of *ANT1* gene expression on *in situ* mitochondrial swelling (visualized by the cobalt-calcein technique) induced by calcimycin in human fibroblasts during various metabolic conditions [+ glucose, no glucose + 2-deoxyglucose (2 mM) + NaCN (5 mM), detailed in the y-axis of the panels]. (**A**) Epifluorescence image of calcein-loaded fibroblasts before induction of mPT. (**B**) Epifluorescence image of the same fibroblasts as shown in panel A, after induction of mPT. (**C**) Time elapsed between calcimycin application and mitochondrial swelling (onset to mPT) detected by wide field imaging of calcein-loaded cultured fibroblasts from the heterozygous mother (ST, black bars) the patient (AF, grey bars), and three control subjects (white bars) during various metabolic conditions, detailed under the x-axis, in the presence of $CoCl_2$. Bars indicate means ± S.E.M. of 29–53 cells from at least 8 different cultures (*$p < 0.05$ significance by ANOVA; p: *e = 0.002, *f = 0.008; cob-calc: cobalt-calcein technique. (**D**) Comparison of mPT-exhibiting and non-exhibiting cells (bricks) in fibroblasts from ST (black bars), AF (grey bars) and control subjects (white bars) with the cobalt-calcein technique, using Fisher exact test.

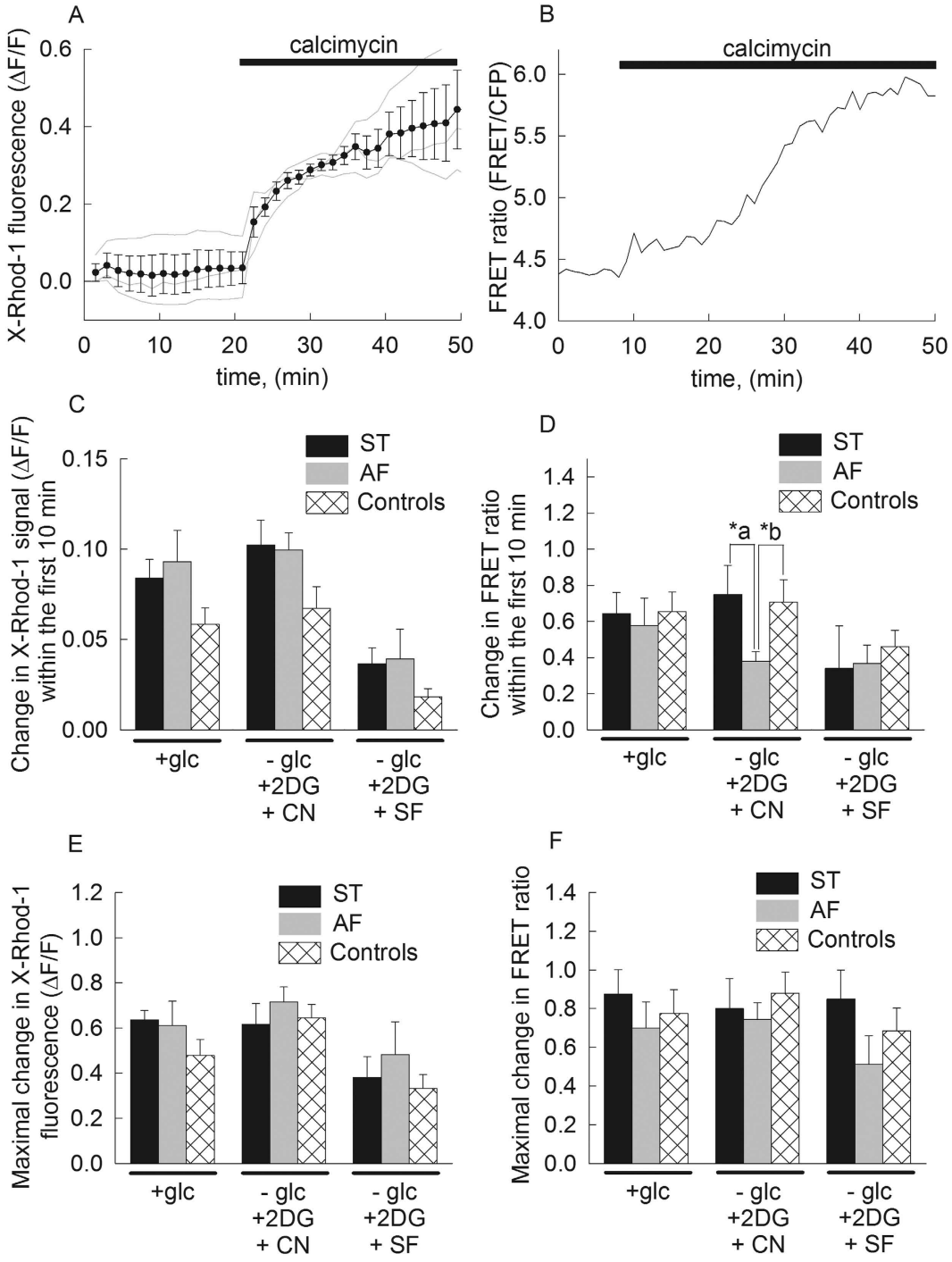

Figure 3. Effect of loss of ANT1 gene expression on matrix Ca^{2+} accumulation upon treatment with calcimycin. (**A**) Representative traces (grey lines) and superimposed mean (black line with S.E.M.) of the effect of calcimycin (2 μM) on mitochondrially-trapped X-Rhod-1 fluorescence, reflecting matrix Ca^{2+} levels. (**B**) Representative trace of the effect of calcimycin (2 μM) on mitochondrially-targeted FRET-based 4mtD3cpv ratio fluorescence, reflecting matrix Ca^{2+} levels. (**C**) Quantification of changes in X-rhod-1 fluorescence within the first 10 min upon addition of calcimycin for various metabolic conditions indicated under the x-axis in cultured fibroblasts from the heterozygous mother (ST, black bars) the patient (AF, grey bars), and three control subjects (pooled cells shown in white hatched bars) during various metabolic conditions, detailed under the x-axis. Bars indicate means ± S.E.M. of 25–40 cells from at least 5 different cultures. (**D**) Quantification of changes in 4mtD3cpv ratio fluorescence within the first 10 min upon addition of calcimycin for various metabolic conditions indicated under the x-axis in cultured fibroblasts from the heterozygous mother (ST, black bars) the patient (AF, grey bars), and three control subjects (pooled cells shown in white hatched bars) during various metabolic conditions, detailed under the x-axis. Bars indicate means ± S.E.M. of 6–10 cells from at least 4 different cultures; p-values: *a = 0.042, *b = 0.044. (**E**) Quantification of maximal changes in X-rhod-1 fluorescence upon addition of calcimycin for various metabolic conditions indicated under the x-axis

in cultured fibroblasts from the heterozygous mother (ST, black bars) the patient (AF, grey bars), and three control subjects (pooled cells shown in white hatched bars) during various metabolic conditions, detailed under the x-axis. Bars indicate means ± S.E.M. of 25–40 cells from at least 5 different cultures. (**F**) Quantification of maximal changes in 4mtD3cpv ratio fluorescence upon addition of calcimycin for various metabolic conditions indicated under the x-axis in cultured fibroblasts from the heterozygous mother (ST, black bars) the patient (AF, grey bars), and three control subjects (pooled cells shown in white hatched bars) during various metabolic conditions, detailed under the x-axis. Bars indicate means ± S.E.M. of 6–10 cells from at least 4 different cultures.

Effect of complete loss of ANT1 gene expression on *in situ* ΔΨm upon treatment with calcimycin. As stated above, the threshold of mPT opening depends on the extent of ΔΨm; de-energization by cyanide in the abscence of glucose would lead to reversal of the mitochondrial ATP synthase in an attempt to maintain membrane potential, at the expense of hydrolysing ATP originating from either cytosol (glycolysis) or mitochondrial substrate-level phosphorylation[46–50]. Thus, during the de-energization protocol and in the presence of calcimycin, a complete collapse of ΔΨm in our cell lines is not warranted and the presence of a residual potential value is more than likely. To address the status of ΔΨm of the various fibroblast cell lines we measured mitochondrial membrane potential by TMRM and distinguishing it from a plasma membrane distribution signal by co-loading with DiBAC4(3), a negatively charged potentiometric dye. Our method is a variant of that described by Gerencser and colleagues[51] which used PMPI instead of DiBAC4(3). We used DiBAC4(3) because it exhibits less spectral overlap with TMRM. Representative epifluorescence images of TMRM and DiBAC4(3) fluorescence representing ΔΨm and plasma membrane potential (ΔΨp) respectively, are shown in Supplemental Fig. 1 during addition of the calibrants (see below); image processing flow of the spectral un-mixing performed as described in[52] is depicted in Supplemental Fig. 2, resulting in the images shown in Fig. 4A. Specifically, the calibration of plasma membrane potential was performed by establishing a K^+-equilibrium potential (K^+ equil) at the plasma membrane followed by stepwise increments of extracellular [K^+] (exact values indicated in panel Fig. 4B,C and Supplemental Fig. 1). The K^+-equilibrium potential was established by the application of 10 μM diazoxide. Finally, a cell membrane calibration cocktail (CDC) was applied. TMRM signals originating from the mitochondrial compartment was then recorded by spectrally un-mixing the DiBAC4(3) fluorescence signal as described in[51] using decomposition algorithms developed in[52].

Representative traces (grey lines) of TMRM fluorescence (spectrally un-mixed from DiBAC4(3) fluorescence, see Supplemental Figs 1 and 2 and details under Materials and Methods) reflecting mitochondrial membrane potential from control fibroblasts under energized conditions are shown in panel Fig. 4D; the mean trace with S.E.M. bars is shown superimposed in black. As shown in panel Fig. 4D, addition of calcimycin decreased TMRM fluorescence by approximately 40%; residual ΔΨm was lost upon further addition of a mitochondrial membrane depolarization cocktail (MDC), the composition of which is detailed under Materials and Methods. From such experiments we evaluated ΔΨm levels in the various cell lines (results obtained from the control cell lines were pooled) during the exact metabolic conditions as indicated for panel Fig. 1F, by taking into account the ratio of calcimycin-induced ($\Delta F_{calcimycin}$) to MDC-induced (ΔF_{total}) change in TMRM fluorescence. The results are summarized in panel Fig. 4E; as shown in panel Fig. 4E, the mitochondrial de-energization induced by calcimycin -in addition to that by cyanide- is highly significantly ($p = 0.001$) greater in AF cells compared to either ST or control cells. Yet, the time lag until onset to mPT (shown in panel Fig. 1F) is greater under the same de-energization conditions for the AF cells. These two results are strongly supportive of the notion that lack of ANT1 renders mitochondria insensitive to modulation of mPT opening by the mitochondrial membrane potential. On the other hand, ΔΨp inferred by DiBAC4(3) fluorescence remained relatively unchanged (<2% changes), panel Fig. 4F. The fact that plasma membrane potential does not show large fluctuations, affords greater assurance that the TMRM signals are almost entirely due to fluctuations of the mitochondrial membrane potential, since TMRM is known to distribute across the plasma membrane as well[53].

Effect of loss of ANT1 gene expression on *in situ* mitochondrial swelling induced by H_2O_2 in human fibroblasts. To address the role of ANT1 on mPT induced by a different than Ca^{2+}-overload stimulus, we subjected the fibroblasts to an oxidant treatment by 1 mM H_2O_2. Reactive oxygen species are known to induce mPT[54]. Just like with calcimycin, treatment of DsRed2-transfected cells with H_2O_2 (without omitting Mg^{2+} from the medium) led to an abrupt change in mitochondrial morphology which by the thinness ratio technique is quantified as swelling, thus implying mPT opening. Representative epifluorescence images of a cell before and after mPT induction are shown in panel Fig. 5A,B, respectively. A time-lapse series of such an experiment is shown in the Supplemental Material (mPT_DsRed2_control_HF_H2O2.avi). A representative thinness ratio trace is shown in panel Fig. 5C, calculated from the recorded time-series images. In the experiments using H_2O_2 as an mPT inducer, we did not variate the metabolic conditions by omitting glucose or including cyanide or uncoupler, because H_2O_2 is expected to exert a considerable metabolic challenge itself[55]. In AF, ST and pooled control subjects' cells, the following parameters were recorded: i) the time elapsed from the addition of H_2O_2 to the appearance of a large magnitude swelling (marked as 'onset to mPT', panel Fig. 5D), and ii) the number of cells exhibiting the large magnitude swelling considered as mPT within the experimental time frame (4 hours in the presence of 1 mM H_2O_2), depicted in panel Fig. 5E.

As shown in panel Fig. 5D, the H_2O_2-induced onset to mPT of *in situ* ST (black bar) mitochondria was similar to that from the control cells (cross-hatched white bar). However, the H_2O_2-induced onset to mPT of *in situ* AF (grey bar) mitochondria was delayed, compared to other cell types. Although this difference is large (~60% further delay in onset to mPT), it was not statistically significantly different from the other cell types but that is

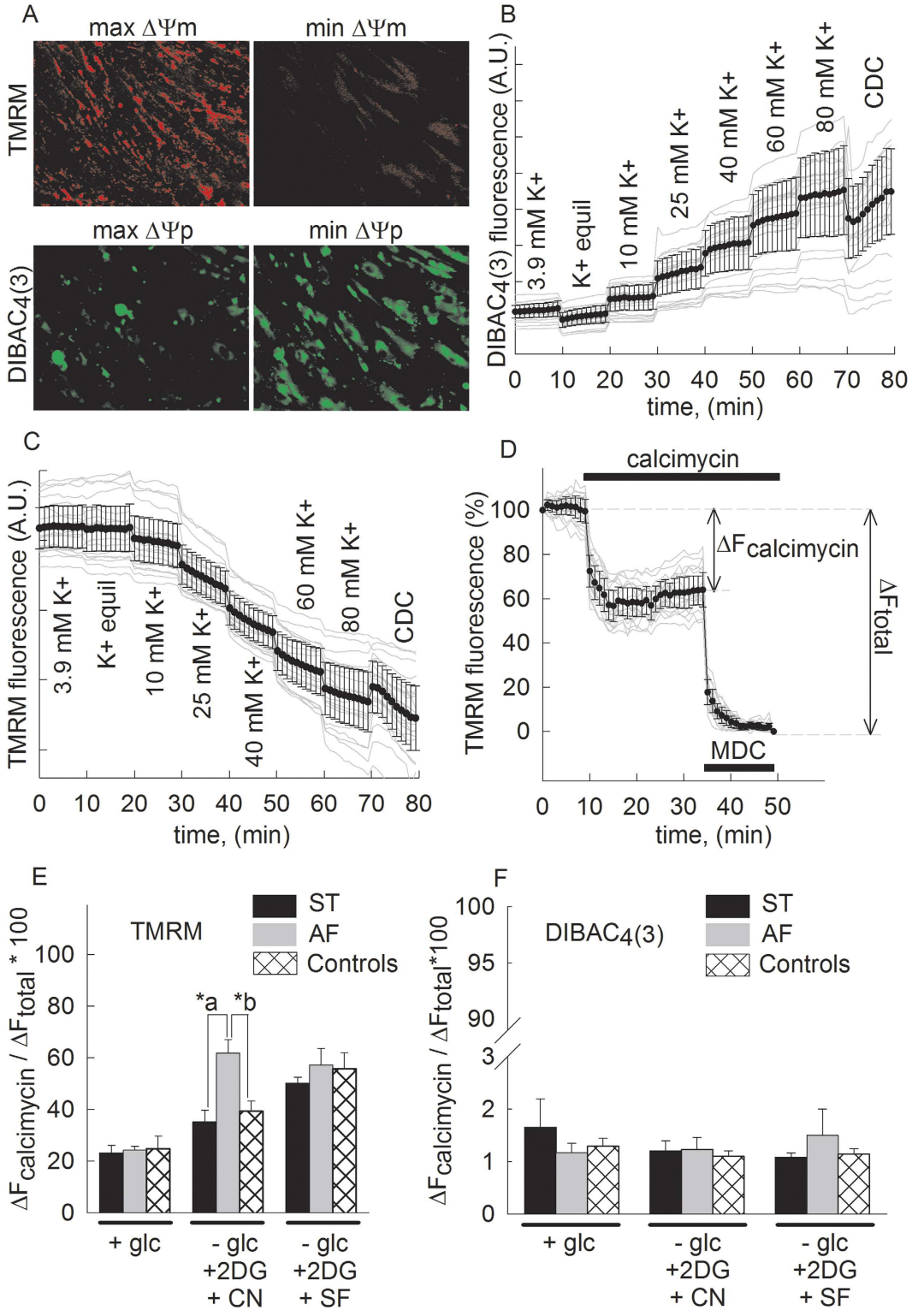

Figure 4. Effect of loss of ANT1 gene expression on *in situ* ΔΨm upon treatment with calcimycin. (**A**) Spectrally un-mixed epifluorescence images of TMRM and $DIBAC_4(3)$ fluorescence representing ΔΨm and ΔΨp respectively; the methodology of spectral un-mixing is outlined in Supplemental Figs 1 and 2. (**B**) $DIBAC_4(3)$ fluorescence traces (grey traces) after spectral un-mixing from TMRM fluorescence bleed-through. $DIBAC_4(3)$ fluorescence intensities (black scatters), indicating mean ± SEM of fluorescence measured over n = 20 fibroblasts (grey lines) in a representative experiment. (**C**) TMRM fluorescence traces after spectral un-mixing from $DIBAC_4(3)$ fluorescence bleed-through (corresponding $DIBAC_4(3)$ fluorescence shown in panel B). TMRM fluorescence intensities (black scatters), indicating mean ± SEM of fluorescence measured over n = 20 fibroblasts (grey lines) from the same experiment, shown in panel B. (**D**) Representative traces (grey lines) and superimposed mean (black line with S.E.M.) of the effect of calcimycin (2 μM) on TMRM fluorescence, spectrally

un-mixed from $DIBAC_4(3)$ fluorescence, reflecting $\Delta\Psi m$. (**E**) Quantification of changes in TMRM fluorescence, spectrally un-mixed from $DIBAC_4(3)$ fluorescence for the various metabolic conditions indicated under the x-axis, for cultured fibroblasts from the heterozygous mother (ST, black bars) the patient (AF, grey bars), and three control subjects (pooled cells shown in white cross-hatched bars). Bars indicate means ± S.E.M. of 168–227 cells from at least 5 different cultures; p-values: *a < 0.001, *b < 0.001. (**F**) Quantification of changes in $DIBAC_4(3)$ fluorescence for the various metabolic conditions indicated under the x-axis, for cultured fibroblasts from the heterozygous mother (ST, black bars) the patient (AF, grey bars), and three control subjects (pooled cells shown in white cross-hatched bars). Bars indicate means ± S.E.M. of 168–227 cells from at least 5 different cultures.

only because a very low number of cells (only three) underwent mPT, reducing the power of statistical analysis. Exactly because of this reason, as shown in panel Fig. 5E, the number of AF cells that underwent mPT was much smaller ($p = 0.0058$) that the other cell types, also leading to not significant differences between AF and control cells evaluated with the Fisher exact test ($p = 0.06$), but yielded significance using the less stringent Chi-square test ($p = 0.029$).

From the above data we concluded that the absence of ANT1 may increase the elapsed time to mPT upon H_2O_2 addition, but most importantly prevent cells from undergoing mPT. These results are in accordance to those by Kokoszka and colleagues[26], where they showed that although tert-butyl hydroperoxide, a non-specific oxidant, and diamide, a specific –SH group oxidant, facilitated isolated mouse liver mitochondria to undergo mPT independent of the presence of ANT, ANT1−/− /ANT2−/− deficient mice exhibited more than three times higher maximum Ca^{2+} uptake capacity compared to wild-type mice[26].

Effect of knocking-down Ant1 expression in C2C12 myotubes on *in situ* mitochondrial swelling induced by calcimycin at different bioenergetic states. In order to evaluate the role of ANT1 on voltage-sensing properties of the mPT in a different cell context, we knocked-down its gene by stably expressing lentiviral shRNA targeted against mouse Ant1 as performed in[56], and swelling of *in situ* mitochondria of these versus scramble RNA (scr) transfected cells were compared during Ca^{2+} overload induced by addition of calcimycin, as a function of various metabolic conditions. As in Kawamata *et al.*[56], ANT1 expression in shRNA-treated cells was undetectable by Western blotting (see panel Fig. 6A), and qPCR for mRNA was reduced by over 90% (not shown). Expression of ANT2 was unaffected, (panel Fig. 6A). *In situ* mitochondria were visualized by wide field epifluorescence imaging of mitochondrially targeted DsRed2. Swelling was monitored by evaluating DsRed2-visualized mitochondrial morphology and changes in mean mitochondrial diameters were calculated using the thinness ratio technique. Representative epifluorescence images before and after induction of mPT are shown in panel Fig. 6B. Time-lapse series of such experiments from an shRNA-transfected and a scramble RNA-transfected C2C12 cell are shown in the Supplemental Material, (mPT_DsRed2_C2C12_shRNA_ANT1.avi, and mPT_DsRed2_C2C12_scramble_ANT1.avi). A representative thinness ratio trace is shown in panel Fig. 6C, calculated from the recorded time-series images. In the experiments performed with shRNA ANT1-transfected and a scramble RNA-transfected C2C12 cells during various metabolic conditions as described in the legend and panels, the following parameters were recorded: i) the time elapsed from the addition of calcimycin to the appearance of a large magnitude swelling (marked as 'onset to mPT', panel Fig. 6D) and ii) the number of cells exhibiting the large magnitude swelling considered as mPT within the experimental time frame (4 hours in the presence of 2 μM calcimycin), depicted in panel Fig. 6E. As shown in panel Fig. 6D, the calcimycin-induced onset to mPT in C2C12 cells with knocked-down ANT1 did not exhibit a statistically significant difference from scramble RNA transfected cells, under any metabolic conditions. However, as shown in panel Fig. 6E, the number of cells exhibiting large-magnitude swelling within the 4 hours of the experimental time frame was statistically significantly different among these cell types when comparing glucose deprivation and NaCN co-application versus no glucose deprivation. Nonetheless, the number of C2C12 cells with knocked-down Ant1 undergoing mPT increased less significantly ($p = 0.0089$ vs $p = 0.0237$) upon chemically-induced hypoxia than cells transfected with scramble RNA. This observation attests to the notion that ANT1 at least partially regulates mPT opening as a function of energization level of *in situ* mitochondria. However, in this experimental setting and just like in human fibroblasts, de-energization by uncoupler did not confer the same alterations in mPT exhibiting versus non-exhibiting cells.

Effect of knocking-down Ant1 expression in permeabilized C2C12 myotubes on the voltage threshold of calcium-induced mPT. We further evaluated the role of ANT1 on the voltage threshold of calcium-induced mPT under various metabolic conditions, in permeabilized C2C12 cells and measuring mitochondrial calcium uptake, $\Delta\Psi m$, and cytochrome c release using the following protocols: i) maximum calcium uptake of *in situ* mitochondria supported by glutamate and malate (panels 7A and 7B, recording calcium uptake and $\Delta\Psi m$, respectively), ii) challenge by submaximal $CaCl_2$ dose followed by titration with step-wise inhibition of respiration by NaCN (50 μM boluses) shown in panels 7C and 7D, recording calcium uptake and $\Delta\Psi m$, respectively, iii) challenge by submaximal $CaCl_2$ dose followed by titration with step-wise dissipation of $\Delta\Psi m$ by SF6847 (10 nM boluses) shown in panels 7E and 7F, recording calcium uptake and $\Delta\Psi m$, respectively, and iv) measuring cytochrome c released from the *in situ* mitochondria of the permeabilized cells during the following time points, indicated in panels 7C and 7E: 1 = before calcium additions, 2 = right after calcium additions, 3 = before loss of sequestered calcium and membrane potential, 4 = after loss of sequestered calcium in scramble RNA treated cells but not shRNA treated cells, 5 = after loss of sequestered calcium and membrane potential in both cells types,

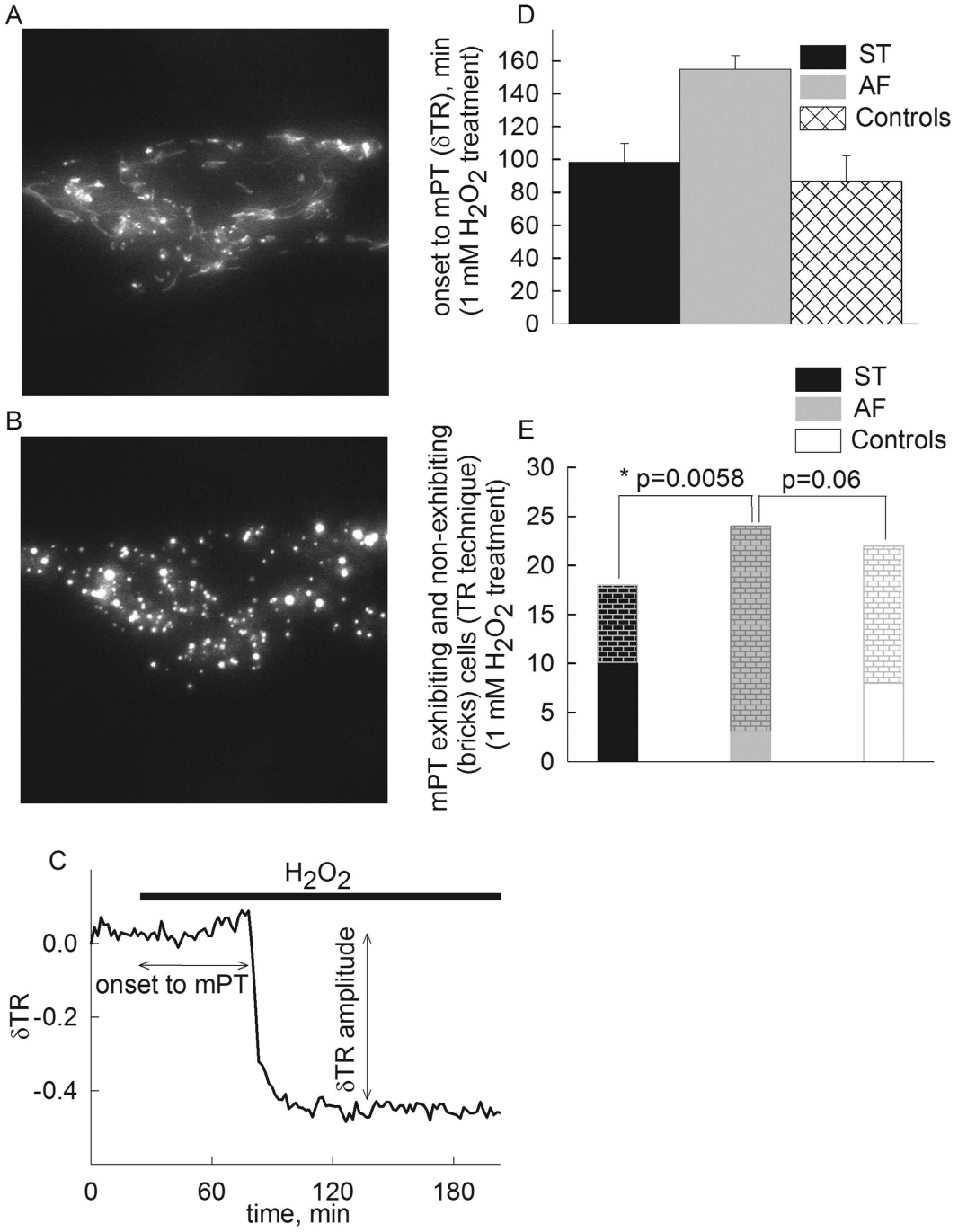

Figure 5. Effect of loss of *ANT1* gene expression on *in situ* mitochondrial swelling (visualized by DsRed2) induced by H_2O_2 in human fibroblasts. (**A**) Epifluorescence image of a fibroblast transfected with DsRed2 before induction of mPT. (**B**) Epifluorescence image of the same fibroblast as shown in panel 5A, after induction of mPT by H_2O_2. (**C**) Representative trace of the effect of H_2O_2 (1 mM) on the thinness ratio (δTR) indicating mitochondrial volume as a function of time. (**D**) Time elapsed between H_2O_2 application and mitochondrial swelling (onset to mPT) detected by wide field imaging of mito-DsRed2 expressed in cultured fibroblasts from the heterozygous mother (ST, black bars) the patient (AF, grey bars), and three control subjects (white cross-hatched bars) in the presence of glucose. The onset to mPT was determined by the sudden increase of mean mitochondrial diameter in the microscopic view field described as a sudden decrease of the thinness ratio (δTR). Bars indicate means ± S.E.M. of 18–24 cells from at least five different cultures. (**E**) Comparison of mPT-exhibiting and non-exhibiting cells (bricks) in fibroblasts from ST (black bars), AF (grey bars) and control subjects (white bars) with the TR technique, using Fisher exact test.

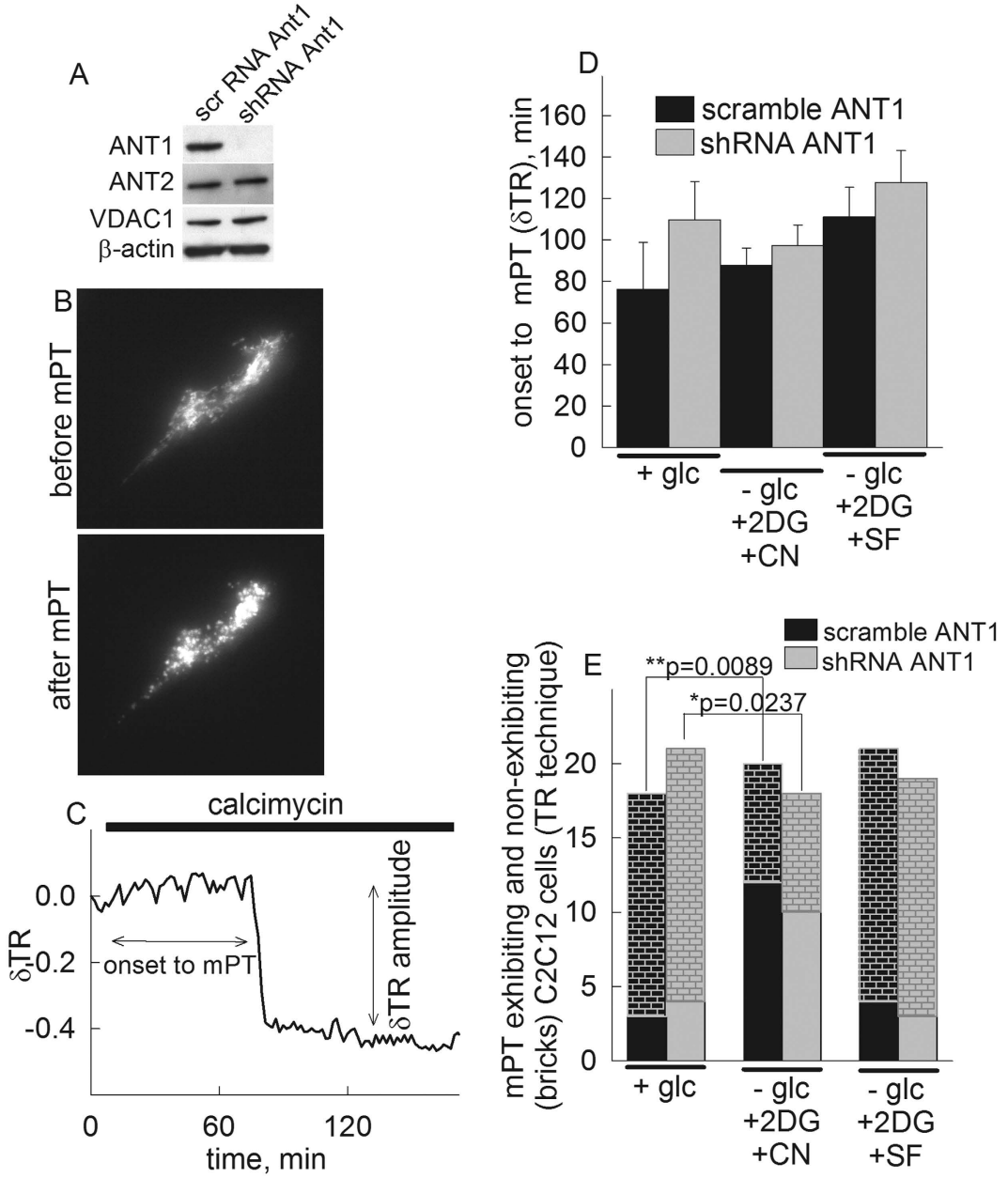

Figure 6. Effect of knocking-down Ant1 in C2C12 myotubes by shRNA using lentiviruses, versus scramble RNA-transfected cells on calcimycin-induced mitochondrial swelling or maximum calcium uptake capacity. (**A**) Scanned images of Western blots of C2C12 myotubes (10 μg loading per lane) transfected with shRNA directed against Ant1 or scramble (scr) RNA, for ANT1, ANT2, VDAC1 and β-actin. (**B**) Epifluorescence image of a C2C12 myotube transfected with DsRed2 before and after induction of mPT. (**C**) Representative trace of the effect of calcimycin (2 μM) on the thinness ratio (δTR) indicating mitochondrial volume as a function of time. (**D**) Time elapsed between calcimycin application and mitochondrial swelling (onset to mPT) detected by wide field imaging of mito-DsRed2 expressed in cultured C2C12 cells treated with shRNA for Ant1 or scramble RNA during various metabolic conditions, detailed under the x-axis. The onset to mPT was determined by the sudden increase of mean mitochondrial diameter in the microscopic view field described as a sudden decrease of the thinness ratio (δTR). Bars indicate means ± S.E.M. of 18–21 cells from at least five different cultures. (**E**) Comparison of mPT-exhibiting and non-exhibiting cells (bricks) detected with the TR technique during various metabolic conditions, using Fisher exact test.

plus a time control for point 5 (cells were probed for cytochrome c release after 20 min of incubation but were not challenged by either $CaCl_2$ or NaCN or uncoupler) and an alamethicin (a pore-forming peptide) control. The amount of cytochrome c appearing in the supernatant upon treatment with alamethicin provides a measure of the maximum amount releasable[57]. Calcium uptake and $\Delta\Psi m$ measurements were performed in parallel but different samples (but from the same cultures) due to spectral overlap of calcium green and safranine O. The assessment of maximum calcium uptake capacity is a widely utilized protocol[58,59], that can be performed in

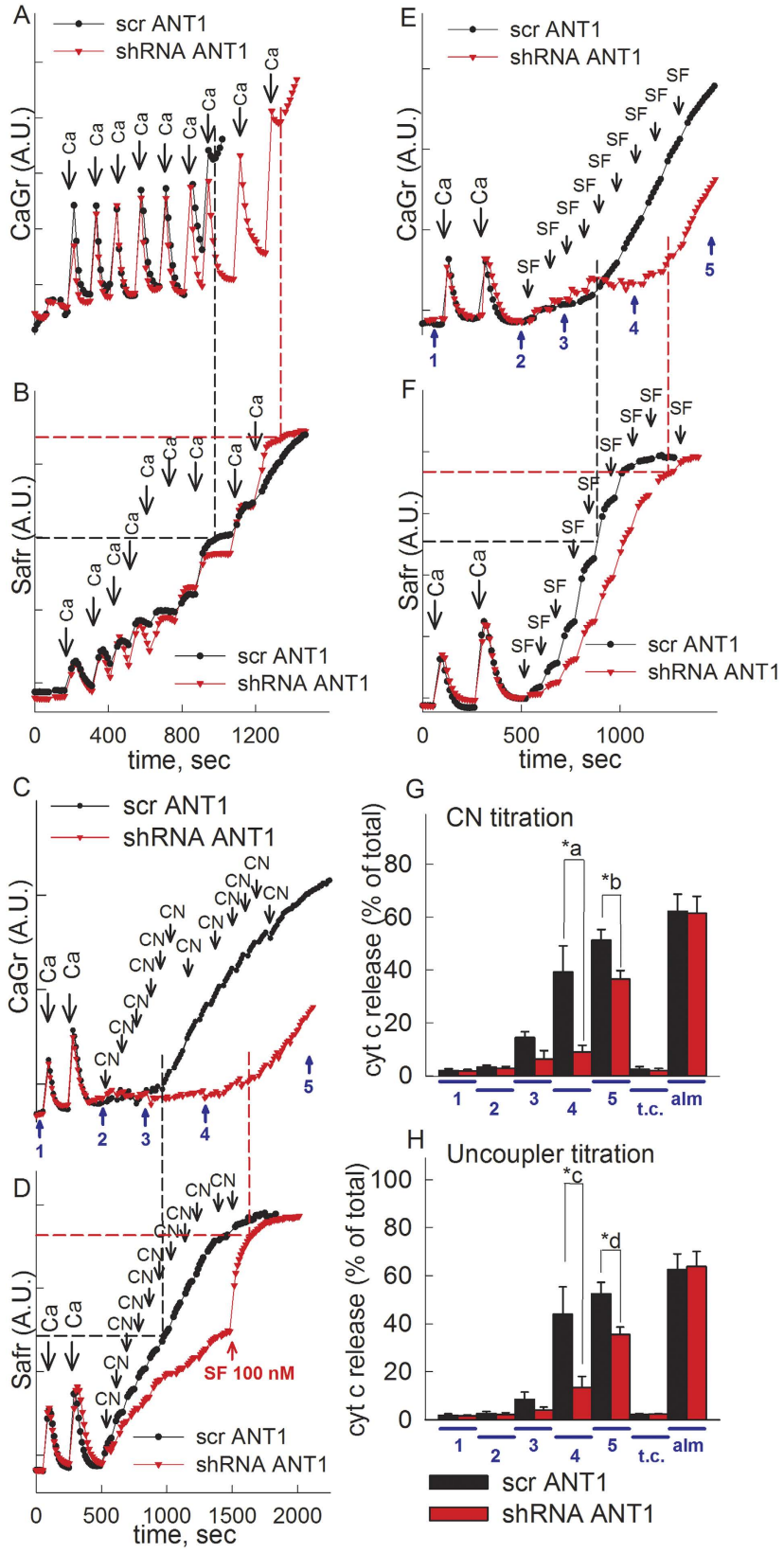

Figure 7. Determination of voltage thresholds of calcium-induced mPT in permeabilized C2C12 cells treated with shRNA for Ant1 (red inverted triangles) or scramble RNA (black closed circles), under various metabolic conditions. (**A**) Maximum calcium uptake capacity in permeabilized C2C12 cells treated with shRNA for Ant1 or scramble RNA. Each addition of $CaCl_2$ (Ca) is 100 μM. (**B**) Safranine O fluorescence traces of C2C12 cells treated exactly as in panel A. Mitochondrial substrates were 5 mM glutamate and 5 mM malate. (**C**) Cells were challenged by two additions of $CaCl_2$ (Ca, 100 μM each) followed by consecutive

additions of 50 μM NaCN, and extramitochondrial calcium was measured by CaGr. Blue numbers and arrows signify time-points of probing for cytochrome c release (see panel **G**). (**D**) Safranine O fluorescence traces of C2C12 cells treated exactly as in panel C, with the exception that shRNA-treated cells received a bolus of 100 nM SF6847 as shown by the red arrow, to indicate that prior to this addition a significant portion of ΔΨm remained. (**E**) Cells were challenged by two additions of $CaCl_2$ (Ca, 100 μM each) followed by consecutive additions of 10 nM SF6847, and extramitochondrial calcium was measured by CaGr. Blue numbers and arrows signify time-points of probing for cytochrome c release (see panel H). (**F**) Safranine O fluorescence traces of C2C12 cells treated exactly as in panel E. All traces shown in panels (A-F) are representative of 5 independent experiments. (**G**) Cytochrome c release (% of the total) estimated by enzyme-linked immunosorbent assay from permeabilized C2C12 cells probed at time points (1–5) indicated in panel C; *a = 0.034, *b = 0.049. (**H**) Cytochrome c release (% of the total) estimated by enzyme-linked immunosorbent assay from permeabilized C2C12 cells probed at time points (1–5) indicated in panel E; *c = 0.047, *d = 0.041. 'Time-controls (t.c.)' signify probing of C2C12 cells at time-point 5 for cytochrome c release that have not been treated with either $CaCl_2$ or NaCN nor SF6847. 'Alm' signifies probing of C2C12 cells for cytochrome c release that have been treated with 80 ngr of alamethicin. Bars indicate means ± S.E.M. of ~270,000 cells from 3 different cultures.

isolated[60], or *in situ* mitochondria of permeabilized cells. In our hands, permeabilized human fibroblasts exhibited a very small maximum mitochondrial calcium uptake capacity, less than 10 nmol/mg protein, and therefore, experiments with these cells were not conducted. On the contrary, permeabilized C2C12 myotubes exhibited very large maximum calcium uptake capacities, providing the opportunity for a more thorough investigation of mPT opening by calcium loading as a function of various metabolic conditions. We have tried to isolate mitochondria from fibroblasts and C2C12 cells, but there were insurmountable obstacles with both cell types; with fibroblasts, an extremely small amount of isolated mitochondria was obtained, not suitable for functional experiments; with C2C12 cells only very harsh homogenization methods could yield sufficient amount of mitochondria, but they were damaged to the extent that they were too leaky for functional studies. For these reasons, we only evaluated C2C12 cells. shRNA-transfected and scramble RNA-transfected C2C12 cells were permeabilized as described under 'Materials and Methods', boluses of 100 μM $CaCl_2$ (panel Fig. 7A,B) were added where indicated, and extramitochondrial Ca^{2+} levels were followed by Calcium Green 5N hexapotassium salt fluorescence (Fig. 7A), or ΔΨm, using safranine O (Fig. 7B). As shown in panel Fig. 7A, C2C12 cells with knocked-down Ant1 exhibited larger mitochondrial calcium uptake capacity than scramble-transfected cells, in the presence of glutamate (5 mM) and malate (5 mM). It is to be noted, that this is not a condition in which mitochondria are continuously fully energized; it is well understood that upon progressive mitochondrial calcium sequestration, mitochondria depolarize accordingly[61]. Indeed, as shown in figure panel 7B, ΔΨm of both cell types gradually dissipates upon increasing calcium load. However, as it is marked by black dashed line for scr RNA-treated cells and red dashed line for shRNA-treated cells, those cells with knocked-down ANT1 expression exhibited loss of sequestered calcium in a much more depolarized ΔΨm range, nearing that of complete depolarization. Next, to obtain a more accurate indication of how mPT opening relates to ΔΨm, we challenged *in situ* mitochondria of permeabilized C2C12 cells with an amount of $CaCl_2$ that is insufficient to trigger pore opening, and then dissipated ΔΨm gradually by inhibiting complex IV with cyanide (50 μM boluses, Fig. 7C,D) or using the uncoupler SF 6847 (10 nM boluses Fig. 7E,F), while recording extramitochondrial Ca^{2+} levels (Fig. 7C,E), or ΔΨm (Fig. 7D,F). In figure panel 7D the addition of 100 nM SF 6847 is also shown (red arrow), signifying that just prior to its addition there was a considerable extent of ΔΨm that could be dissipated. As shown in Fig. 7C–F and marked by black dashed line for scr RNA-treated cells and red dashed line for shRNA-treated cells, those cells with knocked-down ANT1 expression exhibited loss of sequestered calcium in a much more depolarized ΔΨm range, again nearing that of complete depolarization. Furthermore, as shown in figure panels 7G and 7H, a higher percentage of cytochrome c was released from scr RNA treated cells at time points 4 and 5 compared to that from shRNA treated cells, implying that the loss of ΔΨm and sequestered calcium during the same time frame is due to large amplitude swelling resulting in rupture of the outer mitochondrial membrane, implying mPT opening. From these experiments we concluded that ANT1 regulates the voltage threshold of calcium-induced mPT opening.

Effect of complete loss of ANT1 gene expression on ADP-ATP exchange rates as a function of ΔΨm. Human fibroblasts express three (1, 2 and 3) out of the four known isoforms of ANT. *ANT2* was not evaluated particularly for AF and ST cells in ref. 34, therefore we quantified this transcript by qPCR. As shown in panel Fig. 8A, AF cells did not exhibit a statistically significant increase of the *ANT2* gene expression compared to ST and control subject cells. This and the unchanged levels of *ANT3* expression reported in ref. 34 yielded ADP-ATP exchange rates as a function of ΔΨm that did not differ between AF, ST and control subjects' cells, shown in panel Fig. 8B. As reported in ref. 34, AF cells did not express *ANT1* (verified in results shown in panel Fig. 1B,C). From these results we concluded that the differences in onset of the calcimycin-induced mPT between AF, ST and control subjects' cells were unlikely to be attributed to alterations in the adenine nucleotide and/or ΔΨm levels. The determination of the amount of functional ANTs by means of titration with carboxyatractyloside while measuring respiration could not be reliably performed due to the low amount of mitochondria that could be accessed in the permeabilized cultures; this is because the amount of carboxyatractyloside required, was estimated to be in the low nanomolar range, *i.e.* near the K_i of the inhibitor for the ANT (not shown). Neither AF nor ST cells exhibited appreciable ANT reversal rates, probably due to the prominent expression of IF-1 in human fibroblasts[62], also supported by our findings with the cells from three different control subjects, shown in panel figure bB.

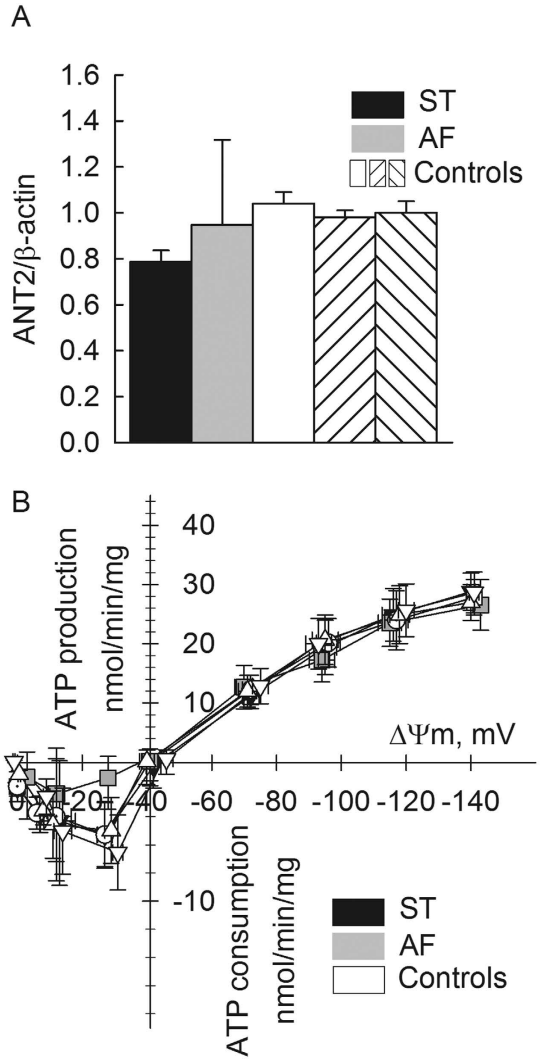

Figure 8. ***ANT2*** **expression and ADP/ATP exchange rates as a function of mitochondrial membrane potential.** (**A**) Reverse transcription PCR and amplification of cDNAs reflecting expression of *ANT2* gene in cultured fibroblasts of the patient (AF), the heterozygous mother (ST) and three control subjects, as a ratio to β-actin expression. (**B**) Plot of ATP–ADP exchange rate mediated by ANT versus ΔΨm in *in situ* mitochondria of AF (grey squares), ST (black squares) and control subjects (white symbols) permeabilized cells depolarized to various voltages by increasing amounts of SF 6847; constructed from the data of 3 independent experiments.

Discussion

mPT is implicated in many human diseases[2,63]. Extensive characterization of the phenomenon has assisted in the recognition of certain proteins as regulatory components, such as cyclophilin D and ANT[1]. VDAC was also initially considered as a structural component, however, tissues engineered to lack all known isoforms still exhibited mPT pore opening and regulation, reviewed in[64]. Furthermore, closure of VDAC hastened mPT pore opening by means of impeding the efflux of superoxide anions from the intermembrane space[65]. Likewise, the outer membrane translocator protein of 18 kDa, TSPO, was originally reported to participate in mPT regulation[66–68], a claim to be recently disproved[69]. Prior to the report that ANT-deficient mice still exhibit the mPT[26], the ANT was already dismissed as a structural element of the pore in dimer formation induced by pore-inducing oxidants[70]; however, formation of ANT dimers need not materialize for pore assembly. Oxidants and other chemical modifiers are known to modulate the mPT; there are at least three sites for oxidation tuning a sensor that translates the changes of both transmembrane voltage and surface potential into changes of the mPT pore open probability[63]. The critical arginines thought to tune the voltage sensor of the pore were considered not to reside in the ANT[18,19]. However, the experiments shown above support the notion that in human fibroblast mitochondria and in C2C12 myotubes the sensor -or at least a part of it- is likely to be isoform 1 of the ANT. Therefore, the sensing property of ANT1 is not mediated through its arginines. The possibility that other oxidation-prone sites tuning the pore sensor reside on ANT1 remains high; indeed, in the presence of oxidants, ANT1$^{-/-}$ /ANT2$^{-/-}$ deficient mice exhibited more than three times higher maximum Ca^{2+} uptake capacity compared to wild-type mice[26].

Most of the experiments by Bernardi's group that proved the inverse correlation of the proton electrochemical gradient to mPT pore opening probability were performed with rat liver mitochondria where ANT2 is the dominant isoform mediating ADP/ATP exchanges, however, in rats ANT1 also exhibits significant expression[71].

ANT1 (but not ANT2) is considered proapoptotic[72]. The proapoptotic property of ANT1 is extremely dominant: overexpression of ANT1 in tumors *in vivo* (where otherwise ANT2 is mostly expressed) induces apoptosis and tumor regression[73]. However, silencing of ANT1 expression in a human glioblastoma cell line induced a paraptotic-like process[74]. On the other hand, overexpression of ANT1 is associated with autosomal dominant facioscapulohumeral muscular dystrophy[75]. In addition, it was shown that mice deficient in ANT1 exhibit increased resistance to excitotoxic insults of the brain[76]. Brain mitochondria from these mice exhibited ~20% higher maximum Ca^{2+} uptake capacity; unfortunately they were not investigated for mPT under de-energized conditions[76].

In[26], WT and ANT1$^{-/-}$/ANT2$^{-/-}$ -deficient mouse liver mitochondria responded equally to uncoupler-induced swelling; we also found no statistically significant difference between ST, control and AF cells, even though there was a trend for AF mitochondria to exhibit smaller 'onset to mPT' values. As a word of caution though: the ANT1$^{-/-}$/ANT2$^{-/-}$ -deficient mice mitochondria exhibited stark differences in bioenergetic parameters and expression levels of other mitochondrial proteins[26], likely the result of compensatory mechanisms, while in this study fibroblasts and C2C12 myotubes were not confounded by other bioenergetic alterations, in line with the results obtained in[34]. However, it is interesting that in AF cells there seems to be a rebound upregulation in ANT2 expression. Since this was observed in Western blots but not Northern blots, it is likely to be due to regulation in the posttranslational modification of the ANT2 protein, and/or its degradation pathway. Relevant to this, different voltage-sensing properties of different ANT isoforms is a possibility. We do acknowledge though that to truly isolate ANT1's functions from possible compensatory effects of other ANT isoforms, re-introduction of expression of ANT isoform 1 in AF cells would prove that only ANT1 is sensitive to alterations of the electrochemical gradient. However, to achieve this, ANT1 level expression should be matched to those observed in the control cell lines, a task posing serious technological challenges.

There is an important difference between de-energization of cells by glucose deprivation and either chemical anoxia, or an uncoupler; in the former, there is no electron flow in the electron transport chain; in the latter, there is high electron flow, despite glucose deprivation due to the presence of endogenous substrates that can fuel the citric acid cycle and yield reducing equivalents. mPT is indeed tuned by a voltage sensor, but in addition to that, electron flow through complex I strongly dictates pore-opening probability[15,77,78] and is maybe part of the voltage-sensing mechanism. Furthermore, there is a potential additional confounding factor regarding the action of uncouplers: mitochondrial Ca^{2+} release by uncouplers is usually ascribed to matrix acidification[79,80], which induces dissociation of the Ca^{2+}phosphate complex. However, matrix acidification by nigericin in the presence of a complete collapse of $\Delta\Psi m$ by combined inhibition of the respiratory chain and the F_0-F_1 ATP synthase, lead to the release of only one-fifth of sequestered calcium[61,81]. Thus, uncouplers exert some other, yet to be identified, effect regarding matrix Ca^{2+} release, which may share a common denominator with induction of the permeability transition.

In the present report we show that in *in situ* mitochondria of ANT1-deficient human fibroblast and C2C12 cells with knocked-down ANT1 by a lentiviral approach, the hastening of Ca^{2+}-induced mPT pore opening during glucose deprivation and chemical anoxia is reduced or abolished. A similar picture emerged from or H_2O_2- treated cells shown to induce mPT opening, with well-documented adverse bioenergetic effects. Finally, voltage-thresholds of calcium-induced mPT opening in permeabilized C2C12 cells were higher if ANT1 was knocked down, than scramble RNA treated cells. We therefore conclude that ANT1 is the module conferring sensitivity of the pore to voltage likely through the electrochemical proton gradient across the inner membrane and/or the electron flow though the electron transport chain. This is in line with previous postulations that ANT either exerts an indirect effect on the mPT by influencing surface potential[82,83], or through altered ANT conformation induced by adenine nucleotide binding affected by membrane potential[32].

Materials and Methods

Cell cultures and transfections. Fibroblast cultures from skin biopsies from the patient with no ANT1 expression (AF) the heterozygous mother (ST) and three control subjects were prepared. All experiments were conducted in accordance with the guidelines of Ethical Rules for Using Human Tissues for Medical Research in Hungary (HM 34/1999) and the Code of Ethics of the World Medical Association (Declaration of Helsinki), and were approved by the Strasbourg University Hospital Ethics Committee. Informed consent was obtained from the patient, her mother, and three healthy donors. Cells were grown on poly-L-ornithine coated 8-well LabTek II chambered coverglasses (Nunc, Rochester, NY, USA) for 2–3 days, at a density of approximately $3*10^5$ cells/well in RPMI1640 medium (GIBCO, Life technologies, Carlsbad, CA, USA) supplemented with 10% fetal bovine serum and 2 mM glutamine and kept at 37 °C in 5% CO_2. The medium was also supplemented with penicillin, streptomycin and amphotericin (item A5955, Sigma-Aldrich St. Louis, MO, USA). Cultures were transfected on the 1st or 2nd DIV with mito-DsRed2 using Lipofectamine 2000 (Life technologies) in RPMI1640 medium at a 3:2 ratio of Lipofectamine (μl) to plasmid DNA (μg) or with mitochondria targeted FRET-based calcium indicator, 4mtD3cpv using flashFECTIN (Oxford Expression Technologies, Oxford, UK) according to the manufacturer's instructions. Experiments were carried out at day 1–2 post transfection. Typical transfection rates were <5% and therefore individual, non-overlapping cells were visualized.

Imaging of cultured cells and estimation of *in situ* mitochondrial swelling with the TR technique. Time lapse epifluorescence microscopy was carried out to image cells expressing mito-DsRed2 at 34 °C and swelling of *in situ* mitochondria was measured by the thinness ratio (TR) technique exactly as described in[44].

Basically, cells were imaged directly on the LabTek chamber without superfusion in a medium containing (in mM): 120 NaCl, 3.5 KCl, 1.3 $CaCl_2$, 20 HEPES, 15 glucose (where indicated) at pH 7.4. Experiments were performed on an Olympus IX81 inverted microscope equipped with a 60 × 1.4 NA oil immersion lens, a Bioprecision-2 *xy*-stage (Ludl Electronic Products Ltd., Hawthorne, NY) and a 75W xenon arc lamp (Lambda LS, Sutter Instruments, Novato, CA). For mito-DsRed2 an 535/20 nm exciter, a 555LP dichroic mirror and an 570LP emitter (Omega Optical, Brattleboro, VT) were used. Time lapses of *z*-series of 16 planes of 512 × 512 pixels frames (digitized at 14bit with no binning, 250 ms exposure time, yielding 0.1 μm pixel size and 0.8 μm *z*-spacing) were acquired using an ORCA-ER2 cooled digital CCD camera (Hamamatsu Photonics, Hamamatsu, Japan) under control of MetaMorph 6.0 software (Molecular Devices; Sunnyvale, CA, USA). The TR technique measures changes of average diameters of thread-like or punctate structures in fluorescence images using a pair of (high and low frequency) bandpass spatial filters. A calibration image series of mito-DsRed2 fluorescence showing mitochondrial swelling by valinomycin (200 nM) was recorded and used to train a spatial bandpass filter set in Image Analyst MKII (Image Analyst Software, Novato, CA). To calculate TR, for each time point the z-stack was mean-intensity projected and the projection image was duplicated. Then, both images were spatially filtered and the absolute value of pixels was taken. The TR was calculated as the ratio of the average fluorescence intensity in the high frequency band pass filtered over the low frequency band pass filtered image. Mitochondrial swelling causes the loss of high spatial frequency image details, therefore a decrease in the TR value. Baseline normalized TR is given as $\delta TR = (TR - TR_0)/TR_0$.

Mitochondrial Ca^{2+} imaging. Two imaging approaches were used: X-Rhod-1 imaging or mitochondria targeted FRET-based calcium indicator, 4mtD3cpv imaging. In X-Rhod-1 experiments cultured cells were loaded with 4 micromole X-Rhod-1-AM for 15 min at 37 °C, in a medium containing (in mM): 120 NaCl, 3.5 KCl, 1.3 $CaCl_2$, 20 HEPES, 15 glucose (where indicated) at pH 7.4, then for 25 min cultures were kept in dark for 'de-esterification'. Experiments were performed at 34 °C on the setup mentioned above with a 60 × 1.4 NA oil immersion lens. For XRhod1 a 535/20 nm exciter, a 555LP dichroic mirror and a 570 LP emitter were used, all from Chroma Technology Corp., Bellows Falls, VT, USA. Time lapses of *z*-series of 5 planes of 1342 × 1024 pixels frames (digitized at 14bit with no binning, 250 ms exposure time, yielding 0.1 μm pixel size and 1.6 μm *z*-spacing) were acquired. For each time point the z-stack was mean-intensity projected. In 4mtD3cpv experiments cultured cells were imaged in a medium containing (in mM): 120 NaCl, 3.5 KCl, 1.3 $CaCl_2$, 20 HEPES, 15 glucose (where indicated) at pH 7.4. Experiments were performed at 34 °C on the setup mentioned above with a 60 × 1.4 NA oil immersion lens. For 4mtD3cpV the following filter sets were used: a 440/20 exciter, a dual bandpass (450–490 nm and 520–560 nm transmitting) dichroic mirror, a 480/10 emitter for CFP (CFP channel) and 535/20 emitter for YFP variant (FRET channel), all from Chroma Technology Corp., Bellows Falls, VT. Time lapses of 1344 × 1024 pixels frames for both channels (digitized at 14 bit with no binning, 400 msec exposure times) were acquired.

Estimation of onset of mPT with the cobalt-calcein technique. Because transfection efficiency with mito-DsRed2 was low, in addition to the thinness ratio technique we assessed onset of mPT implying *in situ* mitochondrial swelling by the cobalt-calcein method, developed by Petronilli *et al.*[43]. Briefly, cells were loaded with 50 nM calcein-AM (above 100 nM, calcein was toxic for these cells) for 20 min at 4 °C, in a medium containing (in mM): 120 NaCl, 3.5 KCl, 1.3 $CaCl_2$, 20 HEPES, 15 glucose (where indicated) at pH 7.4. Subsequently, 1 mM $CoCl_2$ was added, and the LabTek chamber was mounted on the microscope stage. Experiments were performed at 34 °C on the setup mentioned above with a 60 × 1.4 NA oil immersion lens. For calcein an 488/6 nm exciter, a 505LP dichroic mirror and an 535/25 emitter (all from Chroma Technology Corp., Bellows Falls, VT) were used. Time lapses of *z*-series of 5 planes of 1342 × 1024 pixels frames (digitized at 14 bit with no binning, 250 ms exposure time, yielding 0.1 μm pixel size and 1.6 μm *z*-spacing) were acquired. For each time point the z-stack was mean-intensity projected.

Simultaneous measurement of mitochondrial ($\Delta\Psi$m) and plasma membrane potential (PMP). Cultures were incubated at 37°C in imaging medium containing (in mM): 120 NaCl, 3.5 KCl, 1.3 $CaCl_2$, 20 HEPES, 15 glucose (where indicated) at pH 7.4 with TMRM (180 nM) plus the bis-oxonol type plasma membrane potential indicator, $DIBAC_4(3)$ (250 nM, Life Technologies Inc.) for 60 min before the experiment. Experiments were performed at 34 °C on the setup mentioned above with a UAPO 20× air 0.75NA lens. Time lapses of 1342 × 1024 pixels frames (digitized at 12 bit with 4 × 4 binning, 250 msec exposure time for TMRM and 100 msec exposure time for $DIBAC_4(3)$ were acquired. For the illumination of $DIBAC_4(3)$ a 490/10 nm exciter, a 505LP dichroic mirror and 535/25 emission filter were used, for TMRM a 535/20 nm exciter, a 555LP dichroic mirror and a 630/75 emitter were used, all from Chroma Technology Corp., Bellows Falls, VT. The cross-talk of TMRM and $DIBAC_4(3)$ emissions was eliminated by a linear spectral un-mixing algorithm implemented in Image Analyst MKII (Image Analyst Software, Novato, CA) as previously described[51], using decomposition algorithms developed in[52]. The algorithm calculates un-mixed fluorescence intensities by solving a linear equation with the cross-talk coefficient matrix. Coefficient matrix was determined by loading the cultures either with TMRM or $DIBAC_4(3)$ while both emissions (TMRM and $DIBAC_4(3)$) were recorded, see Supplementary Fig. 1. At the end of every experiment, full mitochondrial depolarization and plasma membrane depolarization was achieved by the application of mitochondrial (MDC) and plasma membrane depolarization cocktails (CDC). MDC contained (in μM): 1 valinomycin, 1 SF 6847, 2 oligomycin; CDC contained (in μM): 1 valinomycin, 1 SF 6847, 2 oligomycin, 10 nigericin, 10 monensin.

Northern blotting. Total RNA was isolated using Trizol reagent (Life technologies). RT-PCR was performed with the Phusion RT-PCR kit (Thermo Scientific, Waltham, MA, USA) according to the manufacturer's instructions. Primers (Sigma-Aldrich, St. Louis, MO, USA) were designed using Primer 3[84], and were identical to those used by Le Bras *et al.*[85]. The primers were the following: hANT1-F: ATGGGTGATCACGCTTGGAGCTTCCTAAAG and hANT1-R: TTAGACATATTTTTTGATCTCATCATACAA, hANT2-F: cagcagtctgcctcctcttt and hANT2-R: aagctttgcctccttcatca.

qPCR. Total RNA from the fibroblast cultures was isolated using Trizol reagent (Life technologies). cDNA was synthesized with Oligo d(T)23 VN primer (New England Biolabs, Ipswich, MA, USA) and M-MuLV Reverse Transcriptase (New England Biolabs) as recommended by the manufacturer. Real-time PCR was performed using Power SYBR PCR Mastermix (Life Technologies) and ABI 7900HT Fast Real Time PCR cycler. Primer sequences were obtained from PrimerBank (http://pga.mgh.harvard.edu/primerbank/index.html): ATCACGCTTGGAGCTTCCTAA - ANT1-F, TGCTTCTCAGCACTGATCTGT – ANT1-R; TTATAGACTGCGTGGTCCGTA – ANT2-F; GGCGAAGTTAAGAGCCTGGG – ANT2-R. The results were normalized with the housekeeping human β-actin gene (primers: CTGGCACCCAGCACAATG– HsACTB-F; CCGATCCACACGGAGTACTTG– HsACTB-R[86]). The data were obtained from 3 independent experiments.

Ant1-silenced C2C12 stable cells. Mouse Ant1 in C2C12 cells was silenced with MISSION shRNA lentiviral transduction particles (Sigma, St Louis, MO), as described previously[56]. Briefly, stable cells were created based on the manufacturer's protocol in C2C12 myoblasts and selected with 1 mg/ml puromycin. Scrambled shRNA lentivirus was used to create the control cell line.

Harvesting and permeabilization of cells for ADP-ATP exchange rate measurements and determination of membrane potential. Approximately 1 million fibroblasts (per experiment) cultured as above in poly-L-ornithine coated T-175 cm^2 flasks (Nunc, Rochester, NY, USA) were washed once in phosphate-buffered saline and harvested with 1 ml of 0.25% trypsin-EDTA, inactivated by 9 ml calf serum, followed by centrifugation at 1,100 g for 2 minutes. Next, cells were washed once in ice-cold buffer containing, in mM: KCl 8, K-gluconate 110, NaCl 10, Hepes 10, KH_2PO_4 10, EGTA 0.005, mannitol 10, $MgCl_2$ 1, and 0.5 mg/ml bovine serum albumin (fatty acid-free), pH 7.25 without disturbing the pellet. After the wash, cells were resuspended in 0.2 ml of the same buffer but pre-warmed to 37 °C and also including mitochondrial substrates (5 mM glutamate and 5 mM malate), 25 μM sodium orthovanadate, beryllium trifluoride (see below regarding final concentration) and 50 μM digitonin. Both ADP-ATP exchange rate- and ΔΨm measurements of *in situ* mitochondria in permeabilized cells occurred in this buffer. The rationale for using this particular buffer composition is elaborated in[87,88]. Glutamate and malate were chosen as mitochondrial substrates because they support mitochondrial substrate-level phosphorylation, and as such, they contribute to greater ATP efflux rates[46,49,50].

$[Mg^{2+}]_{free}$ determination from Magnesium Green fluorescence in the experimental volume containing permeabilized fibroblasts and conversion to ADP-ATP exchange rate. ADP-ATP exchange rate was estimated using the recently described fluorimetric method by our laboratory[87], exploiting the differential affinity of ADP and ATP to Mg^{2+}, with the modifications required for digitonin-permeabilized cells, using sodium orthovanadate and beryllium trifluoride, see below and ref. 88. The rate of ATP appearing in the medium following addition of ADP (2 mM) to energized *in situ* mitochondria was calculated from the measured rate of change in free extramitochondrial $[Mg^{2+}]$ using standard binding equations. $[Mg^{2+}]$ in the extramitochondrial environment was measured using the fluorescent indicator, Magnesium Green $5K^+$ salt (1 μM). The assay is designed such that the ANT is the sole mediator of changes in $[Mg^{2+}]_{free}$ in the extramitochondrial volume, as a result of ADP-ATP exchange. For the calculation of [ATP] or [ADP] from $[Mg^{2+}]_{free}$, the apparent K_d values are identical to those in (26) due to identical experimental conditions ($K_{ADP} = 0.906 \pm 0.023$ mM, and $K_{ATP} = 0.114 \pm 0.005$ mM). Magnesium Green fluorescence was recorded in Tecan Infinite® 200 PRO series plate reader (Tecan Deutschland GmbH, Crailsheim, Germany) at a 0.5 Hz acquisition rate, using 505 and 535 nm excitation and emission wavelengths, respectively. Experiments were performed at 37 °C.

Mitochondrial membrane potential (ΔΨm) determination of *in situ* mitochondria of permeabilized cells. ΔΨm was estimated using fluorescence quenching of the cationic dye safranin O due to its accumulation inside energized mitochondria[46], also taking into account the considerations discussed in[89] and[90]. Briefly, ~30,000 C2C12 cells (per experiment) were cultured in 35 mm wells or ~1 million fibroblasts (per experiment) cultured in poly-L-ornithine coated T-175 cm^2 flasks were washed once in phosphate-buffered saline and harvested with 0.25% trypsin-EDTA, inactivated by calf serum, followed by centrifugation at 1,100 g for 2 minutes. Next, cells were washed once in an ice-cold buffer containing, in mM: KCl 8, K-gluconate 110, NaCl 10, Hepes 10, KH_2PO_4 10, EGTA 0.005, mannitol 10, $MgCl_2$ 1, and 0.5 mg/ml bovine serum albumin (fatty acid-free), pH 7.25 without disturbing the pellet. After the wash, cells were resuspended in 0.2 ml of the same buffer but pre-warmed to 37 °C and also including mitochondrial substrates (5 mM glutamate and 5 mM malate), 5 μM safranin O and 50 μM digitonin. For results obtained from fibroblasts, traces obtained from safranin O fluorescence were calibrated to millivolts as described in ref. 50. For results obtained from C2C12 cells, traces are shown as arbitrary units of safranine O fluorescence. Fluorescence was recorded in a Tecan Infinite® 200 PRO series plate reader at a 0.08 Hz acquisition rate, using 495 and 585 nm excitation and emission wavelengths, respectively. After the completion of each experiment, cells were harvested from each well and protein content was determined. Only those data were considered in which protein content variability among wells was <5%. All experiments were performed at 37 °C and in triplicates.

Mitochondrial calcium uptake capacity in permeabilized C2C12 cells. Maximum Ca^{2+} uptake capacity of *in situ mitochondria* of permeabilized cells was estimated as detailed previously[57], with minor modifications: Briefly, approximately 30,000 C2C12 cells (per experiment) were cultured in 35 mm wells, washed once in phosphate-buffered saline and harvested with 0.2 ml of 0.25% trypsin-EDTA, inactivated by 1.8 ml calf serum, followed by centrifugation at 1,100 g for 2 minutes. Next, cells were washed once in an ice-cold buffer containing, in mM: KCl 8, K-gluconate 110, NaCl 10, Hepes 10, KH_2PO_4 10, EGTA 0.005, mannitol 10, $MgCl_2$ 1, and 0.5 mg/ml bovine serum albumin (fatty acid-free), pH 7.25 without disturbing the pellet. After the wash, cells were resuspended in 0.2 ml of the same buffer, but pre-warmed to 37 °C and also including mitochondrial substrates (5 mM glutamate and 5 mM malate), 1 μM Calcium Green 5N hexapotassium salt, (CaGr, Life Technologies) and 50 μM digitonin. Consecutive additions of $CaCl_2$ was added (100 μM boluses) or NaCN (50 μM boluses) or SF6847 (10 or 100 nM boluses) where indicated, until there was no further decrease in CaGr fluorescence, or upon reaching maximum depolarization inferred by parallel measurements of mitochondrial membrane potential measured by safranine O as detailed above. Fluorescence was recorded in a Tecan Infinite® 200 PRO series plate reader at a 0.08 Hz acquisition rate, using 506 and 531 nm excitation and emission wavelengths, respectively. All experiments were performed at 37 °C and in triplicates. After the completion of each experiment, cells were harvested from each well and protein content was determined. Only those data were considered in which protein content variability among wells was $<5\%$.

Western blot analysis. C2C12 cells or human fibroblasts were harvested by trypsinization, washed in phosphate-buffered saline, solubilised in RIPA buffer containing a cocktail of protease inhibitors (Protease Inhibitor Cocktail Set I, Merck Millipore, Billerica, MA, USA) and frozen at −80 °C for further analysis. Frozen pellets were thawed on ice, their protein concentration was determined using the bicinchoninic acid assay as detailed below and separated by sodium dodecyl sulfate – polyacrylamide gel electrophoresis (SDS-PAGE). Separated proteins were transferred to a methanol-activated polyvinylidene difluoride membrane. Immunoblotting was performed as recommended by the manufacturers of the antibodies. Rabbit polyclonal anti-ANT1 (Abcam, Cambridge, UK 1:500 dilution), rabbit polyclonal anti-ANT2 (Biogenesis, UK, 1:500 dilution), rabbit monoclonal anti-VDAC1 (Abcam, 1:5,000 dilution) and mouse monoclonal anti-β actin (Abcam, 1:5,000 dilution) primary antibodies were used. Immunoreactivity was detected using the appropriate peroxidase-linked secondary antibody (1:5,000, donkey anti-rabbit or donkey anti-mouse, Jackson Immunochemicals Europe Ltd, Cambridgeshire, UK) and enhanced chemiluminescence detection reagent (ECL system; Amersham Biosciences GE Healthcare Europe GmbH, Vienna, Austria).

Cytochrome c release. Permeabilized C2C12 cells undergoing calcium uptake capacity determination using CaGr as detailed above were collected at specified time points, and centrifuged at 21,000 g for 3 min. The supernatants were carefully removed, and both the supernatant and pellet fractions were immediately frozen and stored at −20 °C. Cytochrome c immunoreactivity was quantified in both fractions using an enzyme-linked immunosorbent assay kit (Abcam). Before measurement, the supernatant and pellet samples were diluted 1:20 and 1:200, respectively. The release of cytochrome c from *in situ* mitochondria is expressed as the content of cytochrome c in the supernatant as a percentage of the total content of cytochrome c present in the supernatant plus pellet.

Preparation of sodium orthovanadate (Na_3VO_4) and beryllium trifluoride (BeF_3^-). A 25 mM Na_3VO_4 solution was prepared in distilled water (>17 mOhm resistance). The pH of the solution was adjusted to 8.7 with HCl, upon which it turns yellow. This solution was boiled until it turns colorless and cooled to room temperature. The pH was reassessed, and readjusted to pH 8.7 with HCl, upon which the solution turned yellow again. This cycle of boiling until colorless and readjusting the pH was repeated until the solution remains colorless at pH 8.7. Finally, the solution was brought up to the initial volume with distilled water and stored in aliquots at −80 °C. This treatment removes all decavanadate ions present in the Na_3VO_4 solution, which induces mitochondrial membrane depolarization and inhibition of oxygen consumption[91]. The final concentration of orthovanadate used was 12.5 μM. Orthovanadate inhibits the oxidation of only disrupted mammalian mitochondria[92]. Likewise, fluoroberyllium nucleoside diphosphate complexes inhibit only the exposed F_1F_0-ATPase[93]. $BeSO_4$ and NaF are prepared as aqueous solutions of 0.2 M and 0.5 M, respectively, and kept at +4 °C for several years. 0.2 mM BeF_3^- is formed immediately in solution upon mixing of $BeSO_4$ (0.2 mM) and NaF (5 mM). Vanadate, beryllium and fluoride salts are highly toxic to tissues and to the environment, and thus require proper handling and disposal. The combination of orthovanadate and BeF_3^- inhibits kinases, mutases, phosphatases, and ATPases[94,95]. However, some kinases, such as pyruvate kinase, will remain uninhibited[96]. In this respect, upon permeabilization of the cells one has to totally separate pyruvate kinase from its substrate, phosphoenol pyruvate, i.e. there must be no glucose present in the medium prior to permeabilization, and a few minutes lag time must be allowed prior to ADP-ATP exchange rate measurements in order for the remaining reactions by kinases to 'die-out'.

Protein determination. Protein content was measured by the bicinchoninic acid assay[97] using bovine serum albumin protein as standards and calibrating by a 3 parameter power function, $f = y0 + a^*xb$, where y0 is background absorbance in the absence of protein, a and b are constants, and x is the amount of protein in the unknown samples.

Reagents. Standard laboratory chemicals, safranine O and digitonin were from Sigma. Calcium Green 5N $6K^+$ salt, Magnesium Green $5K^+$ salt and calcein-AM were from Life technologies. SF 6847 was from Biomol (BIOMOL GmbH, Hamburg, Germany). Fetal bovine serum was from Atlanta Biologicals (Lawrenceville, GA,

USA) and all other tissue culture reagents were purchased from Life technologies. pDsRed2-mito (mito-DsRed2) was purchased from Clontech (Mountain View, CA). pcDNA-4mtD3cpv was a gift from Amy Palmer & Roger Tsien (Addgene plasmid # 36324).

Statistics. Data are presented as mean ± SEM; significant differences between two groups of data were evaluated by Student's t-test, with $p < 0.05$ considered significant. Significant differences between three or more groups of data were evaluated by one-way analysis of variance followed by Tukey's *post-hoc* analysis, with $p < 0.05$ considered statistically significant. If normality test failed, ANOVA on Ranks was performed.

References

1. Azzolin, L. *et al.* The mitochondrial permeability transition from yeast to mammals. *FEBS Lett.* **584,** 2504–2509 (2010).
2. Bonora, M. *et al.* Molecular mechanisms of cell death: central implication of ATP synthase in mitochondrial permeability transition. *Oncogene* **34,** 1475–1486 (2015).
3. Bonora, M. *et al.* Role of the c subunit of the FO ATP synthase in mitochondrial permeability transition. *Cell Cycle* **12,** 674–683 (2013).
4. Alavian, K. N. *et al.* An uncoupling channel within the c-subunit ring of the F1FO ATP synthase is the mitochondrial permeability transition pore. *Proc. Natl. Acad. Sci. USA* **111,** 10580–10585 (2014).
5. Giorgio, V. *et al.* Dimers of mitochondrial ATP synthase form the permeability transition pore. *Proc. Natl. Acad. Sci. USA* **110,** 5887–5892 (2013).
6. Jonas, E. A., Porter, G. A. Jr., Beutner, G., Mnatsakanyan, N. & Alavian, K. N. Cell death disguised: The mitochondrial permeability transition pore as the c-subunit of the F(1)F(O) ATP synthase. *Pharmacol. Res.* **99,** 382–392 (2015).
7. Halestrap, A. P. The C Ring of the F1Fo ATP Synthase Forms the Mitochondrial Permeability Transition Pore: A Critical Appraisal. *Front Oncol.* **4,** 234, doi: 10.3389/fonc.2014.00234 (2014).
8. Chinopoulos, C. & Szabadkai, G. What makes you can also break you: mitochondrial permeability transition pore formation by the c subunit of the F(1)F(0) ATP-synthase? *Front Oncol.* **3,** 25, doi: 10.3389/fonc.2013.00025 (2013).
9. Szabadkai, G. & Chinopoulos, C. What Makes You Can Also Break You, Part II: Mitochondrial Permeability Transition Pore Formation by Dimers of the F1FO ATP-Synthase? *Front Oncol.* **3,** 140, doi: 10.3389/fonc.2013.00140 (2013).
10. Chinopoulos, C. & Szabadkai, G. What Makes You Can also Break You, Part III: Mitochondrial Permeability Transition Pore Formation by an Uncoupling Channel within the C-Subunit Ring of the F1FO ATP Synthase? *Front Oncol.* **4,** 235, doi: 10.3389/fonc.2014.00235 (2014).
11. Bernardi, P. & von Stockum, S. The permeability transition pore as a Ca(2+) release channel: new answers to an old question. *Cell Calcium* **52,** 22–27 (2012).
12. Bernardi, P. Modulation of the mitochondrial cyclosporin A-sensitive permeability transition pore by the proton electrochemical gradient. Evidence that the pore can be opened by membrane depolarization. *J. Biol. Chem.* **267,** 8834–8839 (1992).
13. Petronilli, V., Cola, C. & Bernardi, P. Modulation of the mitochondrial cyclosporin A-sensitive permeability transition pore. II. The minimal requirements for pore induction underscore a key role for transmembrane electrical potential, matrix pH, and matrix Ca^{2+}. *J. Biol. Chem.* **268,** 1011–1016 (1993).
14. Scorrano, L., Petronilli, V. & Bernardi, P. On the voltage dependence of the mitochondrial permeability transition pore. A critical appraisal. *J. Biol. Chem.* **272,** 12295–12299 (1997).
15. Doczi, J. *et al.* Complex Contribution of Cyclophilin D to Ca^{2+}-induced Permeability Transition in Brain Mitochondria, with Relation to the Bioenergetic State. *J. Biol. Chem.* **286,** 6345–6353 (2011).
16. Petronilli, V. *et al.* The voltage sensor of the mitochondrial permeability transition pore is tuned by the oxidation-reduction state of vicinal thiols. Increase of the gating potential by oxidants and its reversal by reducing agents. *J. Biol. Chem.* **269,** 16638–16642 (1994).
17. Palmeira, C. M. & Wallace, K. B. Benzoquinone inhibits the voltage-dependent induction of the mitochondrial permeability transition caused by redox-cycling naphthoquinones. *Toxicol. Appl. Pharmacol.* **143,** 338–347 (1997).
18. Eriksson, O., Fontaine, E. & Bernardi, P. Chemical modification of arginines by 2,3-butanedione and phenylglyoxal causes closure of the mitochondrial permeability transition pore. *J. Biol. Chem.* **273,** 12669–12674 (1998).
19. Linder, M. D., Morkunaite-Haimi, S., Kinnunen, P. K., Bernardi, P. & Eriksson, O. Ligand-selective modulation of the permeability transition pore by arginine modification. Opposing effects of p-hydroxyphenylglyoxal and phenylglyoxal. *J. Biol. Chem.* **277,** 937–942 (2002).
20. Vesce, S., Jekabsons, M. B., Johnson-Cadwell, L. I. & Nicholls, D. G. Acute glutathione depletion restricts mitochondrial ATP export in cerebellar granule neurons. *J. Biol. Chem.* **280,** 38720–38728 (2005).
21. Majima, E., Shinohara, Y., Yamaguchi, N., Hong, Y. M. & Terada, H. Importance of loops of mitochondrial ADP/ATP carrier for its transport activity deduced from reactivities of its cysteine residues with the sulfhydryl reagent eosin-5-maleimide. *Biochemistry* **33,** 9530–9536 (1994).
22. Costantini, P. *et al.* Oxidation of a critical thiol residue of the adenine nucleotide translocator enforces Bcl-2-independent permeability transition pore opening and apoptosis. *Oncogene* **19,** 307–314 (2000).
23. Michejda, J. & Vignais, P. V. The energy-dependent unmasking of -SH groups in the mitochondrial ADP/ATP carrier, and its prevention by nigericin. *FEBS Lett.* **132,** 129–132 (1981).
24. Halestrap, A. P. & Brenner, C. The adenine nucleotide translocase: a central component of the mitochondrial permeability transition pore and key player in cell death. *Curr. Med. Chem.* **10,** 1507–1525 (2003).
25. Zoratti, M. & Szabo, I. The mitochondrial permeability transition. *Biochim. Biophys. Acta* **1241,** 139–176 (1995).
26. Kokoszka, J. E. *et al.* The ADP/ATP translocator is not essential for the mitochondrial permeability transition pore. *Nature* **427,** 461–465 (2004).
27. Menze, M. A., Hutchinson, K., Laborde, S. M. & Hand, S. C. Mitochondrial permeability transition in the crustacean Artemia franciscana: absence of a calcium-regulated pore in the face of profound calcium storage. *Am. J. Physiol Regul. Integr. Comp Physiol* **289,** R68–R76 (2005).
28. Konrad, C. *et al.* A distinct sequence in the adenine nucleotide translocase from Artemia franciscana embryos is associated with insensitivity to bongkrekate and atypical effects of adenine nucleotides on Ca(2+) uptake and sequestration. *FEBS J.* **278,** 822–836 (2011).
29. Klingenberg, M. The ADP and ATP transport in mitochondria and its carrier. *Biochim. Biophys. Acta* **1778,** 1978–2021 (2008).
30. Konrad, C., Kiss, G., Torocsik, B., Adam-Vizi, V. & Chinopoulos, C. Absence of Ca^{2+}-induced mitochondrial permeability transition but presence of bongkrekate-sensitive nucleotide exchange in C. crangon and P. serratus. *Plos. ONE.* **7,** e39839, doi: 10.1371/journal.pone.0039839 (2012).
31. Wysocka-Kapcinska, M. *et al.* The suppressor of AAC2 Lethality SAL1 modulates sensitivity of heterologously expressed artemia ADP/ATP carrier to bongkrekate in yeast. *Plos. ONE* **8,** e74187, doi: 10.1371/journal.pone.0074187 (2013).

32. Halestrap, A. P., Woodfield, K. Y. & Connern, C. P. Oxidative stress, thiol reagents, and membrane potential modulate the mitochondrial permeability transition by affecting nucleotide binding to the adenine nucleotide translocase. *J. Biol. Chem.* **272,** 3346–3354 (1997).
33. McStay, G. P., Clarke, S. J. & Halestrap, A. P. Role of critical thiol groups on the matrix surface of the adenine nucleotide translocase in the mechanism of the mitochondrial permeability transition pore. *Biochem. J.* **367,** 541–548 (2002).
34. Echaniz-Laguna, A. *et al.* Complete loss of expression of the ANT1 gene causing cardiomyopathy and myopathy. *J. Med. Genet.* **49,** 146–150 (2012).
35. Abramov, A. Y. & Duchen, M. R. Actions of ionomycin, 4-BrA23187 and a novel electrogenic Ca^{2+} ionophore on mitochondria in intact cells. *Cell Calcium* **33,** 101–112 (2003).
36. Yun, B. *et al.* Serine hydrolase inhibitors block necrotic cell death by preventing calcium overload of the mitochondria and permeability transition pore formation. *J. Biol. Chem* **289,** 1491–1504 (2014).
37. Wang, Z., Cai, F., Hu, L. & Lu, Y. The role of mitochondrial permeability transition pore in regulating the shedding of the platelet GPIbalpha ectodomain. *Platelets.* **25,** 373–381 (2014).
38. Kahraman,S., Bambrick, L. L. & Fiskum, G. Effects of FK506 and cyclosporin a on calcium ionophore-induced mitochondrial depolarization and cytosolic calcium in astrocytes and neurons. *J. Neurosci. Res.* **89,** 1973–1978 (2011).
39. Dumas, J. F. *et al.* Effect of transient and permanent permeability transition pore opening on NAD(P)H localization in intact cells. *J. Biol. Chem* **284,** 15117–15125 (2009).
40. Oh, K. W., Qian, T., Brenner, D. A. & Lemasters, J. J. Salicylate enhances necrosis and apoptosis mediated by the mitochondrial permeability transition. *Toxicol. Sci.* **73,** 44–52 (2003).
41. Beavis, A. D. Properties of the inner membrane anion channel in intact mitochondria. *J. Bioenerg. Biomembr.* **24,** 77–90 (1992).
42. Beavis, A. D., Lu, Y. & Garlid, K. D. On the regulation of K^+ uniport in intact mitochondria by adenine nucleotides and nucleotide analogs. *J. Biol. Chem* **268,** 997–1004 (1993).
43. Petronilli,V. *et al.* Transient and long-lasting openings of the mitochondrial permeability transition pore can be monitored directly in intact cells by changes in mitochondrial calcein fluorescence. *Biophys. J.* **76,** 725–734 (1999).
44. Gerencser, A. A., Doczi, J., Torocsik, B., Bossy-Wetzel,E. & Adam-Vizi, V. Mitochondrial swelling measurement *in situ* by optimized spatial filtering: astrocyte-neuron differences. *Biophys. J.* **95,** 2583–2598 (2008).
45. Palmer, A. E. *et al.* Ca^{2+} indicators based on computationally redesigned calmodulin-peptide pairs. *Chem Biol.* **13,** 521–530 (2006).
46. Chinopoulos, C. *et al.* Forward operation of adenine nucleotide translocase during F0F1-ATPase reversal: critical role of matrix substrate-level phosphorylation. *FASEB J.* **24,** 2405–2416 (2010).
47. Chinopoulos, C. The "B Space" of mitochondrial phosphorylation. *J. Neurosci. Res.* **89,** 1897–1904 (2011).
48. Chinopoulos, C. Mitochondrial consumption of cytosolic ATP: not so fast. *FEBS Lett.* **585,** 1255–1259 (2011).
49. Kiss, G. *et al.* The negative impact of alpha-ketoglutarate dehydrogenase complex deficiency on matrix substrate-level phosphorylation. *FASEB J.* **27,** 2392–2406 (2013).
50. Kiss, G. *et al.* Mitochondrial diaphorases as NAD(+) donors to segments of the citric acid cycle that support substrate-level phosphorylation yielding ATP during respiratory inhibition. *FASEB J.* **28,** 1682–1697 (2014).
51. Gerencser, A. A. *et al.* Quantitative measurement of mitochondrial membrane potential in cultured cells: calcium-induced de- and hyperpolarization of neuronal mitochondria. *J. Physiol* **590,** 2845–2871 (2012).
52. Neher, R. A. *et al.* Blind source separation techniques for the decomposition of multiply labeled fluorescence images. *Biophys. J.* **96,** 3791–3800 (2009).
53. Ward, M. W., Rego, A. C., Frenguelli, B. G. & Nicholls, D. G. Mitochondrial membrane potential and glutamate excitotoxicity in cultured cerebellar granule cells. *J. Neurosci.* **20,** 7208–7219 (2000).
54. Halestrap, A. P. & Richardson, A. P. The mitochondrial permeability transition: a current perspective on its identity and role in ischaemia/reperfusion injury. *J. Mol. Cell Cardiol.* **78,** 129–141 (2015).
55. Chinopoulos, C., Tretter, L. & Adam-Vizi, V. Depolarization of *in situ* mitochondria due to hydrogen peroxide-induced oxidative stress in nerve terminals: inhibition of alpha-ketoglutarate dehydrogenase. *J. Neurochem.* **73,** 220–228 (1999).
56. Kawamata, H., Tiranti, V., Magrane, J., Chinopoulos, C. & Manfredi,G. adPEO mutations in ANT1 impair ADP-ATP translocation in muscle mitochondria. *Hum. Mol. Genet.* **20,** 2964–2974 (2011).
57. Chinopoulos, C., Starkov, A. A. & Fiskum, G. Cyclosporin A-insensitive permeability transition in brain mitochondria: inhibition by 2-aminoethoxydiphenyl borate. *J. Biol. Chem.* **278,** 27382–27389 (2003).
58. Kristian, T., Weatherby, T. M., Bates, T. E. & Fiskum, G. Heterogeneity of the calcium-induced permeability transition in isolated non-synaptic brain mitochondria. *J. Neurochem.* **83,** 1297–1308 (2002).
59. Murphy, A. N., Bredesen, D. E., Cortopassi, G., Wang, E. & Fiskum,G. Bcl-2 potentiates the maximal calcium uptake capacity of neural cell mitochondria. *Proc. Natl. Acad. Sci. USA* **93,** 9893–9898 (1996).
60. Marcu, R., Neeley, C. K., Karamanlidis, G. & Hawkins, B. J. Multi-parameter measurement of the permeability transition pore opening in isolated mouse heart mitochondria. *J. Vis. Exp.* **67,** 4131, doi: 10.3791/4131 (2012).
61. Chinopoulos, C. & Adam-Vizi, V. Mitochondrial Ca^{2+} sequestration and precipitation revisited. *FEBS J.* **277,** 3637–3651 (2010).
62. Das, A. M., Byrd,D. J. & Brodehl, J. Regulation of the mitochondrial ATP-synthase in human fibroblasts. *Clin. Chim. Acta* **231,** 61–68 (1994).
63. Rasola, A. & Bernardi, P. The mitochondrial permeability transition pore and its involvement in cell death and in disease pathogenesis. *Apoptosis.* **12,** 815–833 (2007).
64. Bernardi, P. The mitochondrial permeability transition pore: a mystery solved? *Front Physiol* **4,** 95, doi: 10.3389/fphys.2013.00095 (2013).
65. Tikunov, A. *et al.* Closure of VDAC causes oxidative stress and accelerates the Ca(2+)-induced mitochondrial permeability transition in rat liver mitochondria. *Arch. Biochem. Biophys.* **495,** 174–181 (2010).
66. Roy, S. S. *et al.* Bad targets the permeability transition pore independent of Bax or Bak to switch between Ca^{2+}-dependent cell survival and death. *Mol. Cell* **33,** 377–388 (2009).
67. Sileikyte, J. *et al.* Regulation of the inner membrane mitochondrial permeability transition by the outer membrane translocator protein (peripheral benzodiazepine receptor). *J. Biol. Chem.* **286,** 1046–1053 (2011).
68. Batarseh, A. & Papadopoulos, V. Regulation of translocator protein 18 kDa (TSPO) expression in health and disease states. *Mol. Cell Endocrinol.* **327,** 1–12 (2010).
69. Sileikyte, J. *et al.* Regulation of the mitochondrial permeability transition pore by the outer membrane does not involve the peripheral benzodiazepine receptor (Translocator Protein of 18 kDa (TSPO)). *J. Biol. Chem* **289,** 13769–13781 (2014).
70. Costantini, P., Colonna, R. & Bernardi, P. Induction of the mitochondrial permeability transition by N-ethylmaleimide depends on secondary oxidation of critical thiol groups. Potentiation by copper-ortho-phenanthroline without dimerization of the adenine nucleotide translocase. *Biochim. Biophys. Acta* **1365,** 385–392 (1998).
71. Dorner, A., Olesch, M., Giessen, S., Pauschinger, M. & Schultheiss, H. P. Transcription of the adenine nucleotide translocase isoforms in various types of tissues in the rat. *Biochim. Biophys. Acta* **1417,** 16–24 (1999).
72. Bauer, M. K., Schubert, A., Rocks, O. & Grimm, S. Adenine nucleotide translocase-1, a component of the permeability transition pore, can dominantly induce apoptosis. *J. Cell Biol.* **147,** 1493–1502 (1999).
73. Jang, J. Y., Choi,Y., Jeon, Y. K., Aung, K. C. & Kim, C. W. Over-expression of adenine nucleotide translocase 1 (ANT1) induces apoptosis and tumor regression *in vivo*. *BMC. Cancer* **8,** 160, doi: 10.1186/1471-2407-8-160 (2008).

74. Lena, A. *et al.* The silencing of adenine nucleotide translocase isoform 1 induces oxidative stress and programmed cell death in ADF human glioblastoma cells. *FEBS J.* **277,** 2853–2867 (2010).
75. Laoudj-Chenivesse, D. *et al.* Increased levels of adenine nucleotide translocator 1 protein and response to oxidative stress are early events in facioscapulohumeral muscular dystrophy muscle. *J. Mol. Med.* (*Berl*) **83,** 216–224 (2005).
76. Lee, J., Schriner, S. E. & Wallace, D. C. Adenine nucleotide translocator 1 deficiency increases resistance of mouse brain and neurons to excitotoxic insults. *Biochim. Biophys. Acta* **1787,** 364–370 (2009).
77. Fontaine, E., Eriksson, O., Ichas, F. & Bernardi, P. Regulation of the permeability transition pore in skeletal muscle mitochondria. Modulation By electron flow through the respiratory chain complex i. *J. Biol. Chem.* **273,** 12662–12668 (1998).
78. Fontaine, E. & Bernardi, P. Progress on the mitochondrial permeability transition pore: regulation by complex I and ubiquinone analogs. *J. Bioenerg. Biomembr.* **31,** 335–345 (1999).
79. Chalmers, S. & Nicholls, D. G. The relationship between free and total calcium concentrations in the matrix of liver and brain mitochondria. *J. Biol. Chem.* **278,** 19062–19070 (2003).
80. Nicholls, D. G. & Chalmers, S. The integration of mitochondrial calcium transport and storage. *J. Bioenerg. Biomembr.* **36,** 277–281 (2004).
81. Vajda, S. *et al.* A re-evaluation of the role of matrix acidification in uncoupler-induced Ca^{2+} release from mitochondria. *FEBS J.* **276,** 2713–2724 (2009).
82. Bernardi, P., Broekemeier, K. M. & Pfeiffer,D. R. Recent progress on regulation of the mitochondrial permeability transition pore; a cyclosporin-sensitive pore in the inner mitochondrial membrane. *J. Bioenerg. Biomembr.* **26,** 509–517 (1994).
83. Broekemeier, K. M. & Pfeiffer, D. R. Inhibition of the mitochondrial permeability transition by cyclosporin A during long time frame experiments: relationship between pore opening and the activity of mitochondrial phospholipases. *Biochemistry* **34,** 16440–16449 (1995).
84. Rozen, S. & Skaletsky, H. Primer3 on the WWW for general users and for biologist programmers. *Methods Mol. Biol.* **132,** 365–386 (2000).
85. Le, B. M. *et al.* Chemosensitization by knockdown of adenine nucleotide translocase-2. *Cancer Res.* **66,** 9143–9152 (2006).
86. Vilchez, D. *et al.* Increased proteasome activity in human embryonic stem cells is regulated by PSMD11. *Nature* **489,** 304–308 (2012).
87. Chinopoulos, C. *et al.* A novel kinetic assay of mitochondrial ATP-ADP exchange rate mediated by the ANT. *Biophys. J.* **96,** 2490–2504 (2009).
88. Kawamata, H., Starkov, A. A., Manfredi, G. & Chinopoulos, C. A kinetic assay of mitochondrial ADP-ATP exchange rate in permeabilized cells. *Anal. Biochem.* **407,** 52–57 (2010).
89. Perevoshchikova, I. V., Sorochkina, A. I., Zorov, D. B. & Antonenko, Y. N. Safranine O as a fluorescent probe for mitochondrial membrane potential studied on the single particle level and in suspension. *Biochemistry* (*Mosc.*) **74,** 663–671 (2009).
90. Figueira, T. R., Melo, D. R., Vercesi, A. E. & Castilho, R. F. Safranine as a fluorescent probe for the evaluation of mitochondrial membrane potential in isolated organelles and permeabilized cells. *Methods Mol. Biol.* **810,** 103–117 (2012).
91. Aureliano, M. & Crans, D. C. Decavanadate (V10 O28 6-) and oxovanadates: oxometalates with many biological activities. *J. Inorg. Biochem.* **103,** 536–546 (2009).
92. Byczkowski, J., Zychlinski, L. & Tluczkiewicz, J. Interaction of vanadate with respiratory chain of rat liver and wheat seedling mitochondria. *Int. J. Biochem.* **10,** 1007–1011 (1979).
93. Issartel, J. P., Dupuis, A., Lunardi, J. & Vignais, P. V. Fluoroaluminum and fluoroberyllium nucleoside diphosphate complexes as probes of the enzymatic mechanism of the mitochondrial F1-ATPase. *Biochemistry* **30,** 4726–4733 (1991).
94. Ray, B. D., Moore, J. M. & Rao, B. D. 31P NMR studies of enzyme-bound substrate complexes of yeast 3-phosphoglycerate kinase: III. Two ADP binding sites and their Mg(II) affinity; effects of vanadate and arsenate on enzymic complexes with ADP and 3-P-glycerate. *J. Inorg. Biochem.* **40,** 47–57 (1990).
95. Climent, F., Bartrons, R., Pons, G. & Carreras, J. Effect of vanadate on phosphoryl transfer enzymes involved in glucose metabolism. *Biochem. Biophys. Res. Commun.* **101,** 570–576 (1981).
96. Lord, K. A. & Reed, G. H. Vanadyl(IV) complexes with pyruvate kinase: activation of the enzyme and electron paramagnetic resonance properties of ternary complexes with the protein. *Arch. Biochem. Biophys.* **281,** 124–131 (1990).
97. Smith, P. K. *et al.* Measurement of protein using bicinchoninic acid. *Anal. Biochem.* **150,** 76–85 (1985).

Acknowledgements

We thank Katalin Zölde for excellent technical assistance. This work was supported by Országos Tudományos Kutatási Alapprogramok (OTKA) [112230] grant and Magyar Tudományos Akadémia (MTA) [02001] grant and the Hungarian Brain Research Program [KTIA_13_NAP-A-III/6] grant to V.A-V., grants TÁMOP [4.2.1./B-09/1/KMR] and [NAP-A] to M.J.M. and A.G., grant NIH/NIA [AG014930] to A.A.S., and grants MTA-SE Lendület Neurobiochemistry Research Division [95003], OTKA NNF [78905], OTKA NNF2 [85658], OTKA K [100918] and Egészségügyi Tudományos Tanács [55160] to C. C.

Author Contributions

J.D., B.T., A.E.-L., B.M.C., A.S., N.S., A.G., H.K. and C.C. performed the experiments, analyzed and interpreted data; M.J.M., G.M., V.A.-V. and C.C. edited the manuscript; C.C. designed the experiments and wrote the manuscript. All authors reviewed the manuscript.

Additional Information

Supplementary information accompanies this paper at http://www.nature.com/srep

Competing financial interests: The authors declare no competing financial interests.

How to cite this article: Doczi, J. *et al.* Alterations in voltage-sensing of the mitochondrial permeability transition pore in ANT1-deficient cells. *Sci. Rep.* **6**, 26700; doi: 10.1038/srep26700 (2016).

This work is licensed under a Creative Commons Attribution 4.0 International License. The images or other third party material in this article are included in the article's Creative Commons license, unless indicated otherwise in the credit line; if the material is not included under the Creative Commons license, users will need to obtain permission from the license holder to reproduce the material. To view a copy of this license, visit http://creativecommons.org/licenses/by/4.0/